Identification of an endocannabinoid gut-brain vagal mechanism controlling food reward and energy homeostasis

Chloe Berland, Julien Castel, Romano Terrasi, Enrica Montalban, Ewout Foppen, Claire Martin, Giulio G. Muccioli, Serge Luquet, Giuseppe Gangarossa

Identification of an endocannabinoid gut-brain vagal mechanism controlling food reward and energy homeostasis

Chloé Berland, Julien Castel, Enrica Montalban, Ewout Foppen, Claire Martin, Giulio G Muccioli, Serge Luquet, Giuseppe Gangarossa

Identification of an endocannabinoid gut-brain vagal mechanism controlling food reward and energy homeostasis

Chloé Berland[1], Julien Castel[1], Enrica Montalban[1], Ewout Foppen[1], Claire Martin[1], Giulio G. Muccioli[2], Serge Luquet[1], Giuseppe Gangarossa[1]

[1] Université de Paris, BFA, UMR 8251, CNRS, F-75013 Paris, France

[2] Bioanalysis and Pharmacology of Bioactive Lipids Research Group, Louvain Drug Research Institute, Université catholique de Louvain, 1200 Brussels, Belgium

Correspondence to: giuseppe.gangarossa@u-paris.fr (GG, @PeppeGanga)

Key words: binge eating, dopamine, 2-AG, vagus nerve, striatum, reward, metabolism

Abstract (234)

The regulation of food intake, a *sine qua non* requirement for survival, thoroughly shapes feeding and energy balance by integrating both homeostatic and hedonic values of food. Unfortunately, the widespread access to palatable food has led to the development of feeding habits that are independent from metabolic needs. Among these, binge eating (BE) is characterized by uncontrolled voracious eating. While reward deficit seems to be a major contributor of BE, the physiological and molecular underpinnings of BE establishment remain elusive. Here, we combined a physiologically relevant BE mouse model with multiscale *in vivo* integrative approaches to explore the functional connection between the gut-brain axis and the reward and homeostatic brain structures.

Our results show that BE elicits compensatory adaptations requiring the gut-to-brain axis which, through the vagus nerve, relies on the permissive actions of peripheral endocannabinoids (eCBs) signaling. Selective inhibition of peripheral CB1 receptors resulted in a vagus-dependent increased hypothalamic activity, modified metabolic efficiency, and dampened activity of mesolimbic dopamine circuit, altogether leading to the suppression of palatable eating. We provide compelling evidence for a yet unappreciated physiological integrative mechanism by which variations of peripheral eCBs control the activity of the vagus nerve, thereby in turn gating the additive responses of both homeostatic and hedonic brain circuits which govern homeostatic and reward-driven feeding.

In conclusion, we reveal that vagus-mediated eCBs/CB1R functions represent an interesting and innovative target to modulate energy balance and food-reward disorders.

Introduction

Feeding is a complex and highly conserved process whose orchestration results from the dynamic integration of homeostatic and hedonic signals (Lutter and Nestler, 2009; Rossi and Stuber, 2018; Saper et al., 2002). While the firsts can be broadly defined as key regulators of food intake to ensure optimal energy balance, the seconds mainly relate to the reinforcing properties of sensory stimuli (perception, cues, taste, odors) and reward-associated features of feeding. The homeostatic and hedonic components of feeding have been respectively attributed to the hypothalamic and the reward systems (Berthoud et al., 2017). However, despite the well-accepted recognition that both feeding components are tightly and functionally interconnected (Berthoud et al., 2017), they have usually been investigated as isolated systems: homeostatic feeding *vs* hedonic feeding (Rossi and Stuber, 2018). In addition, the counterpointing central *vs* peripheral regulations of feeding add a supplemental degree of complexity in the identification of integrative regulatory mechanisms (Coll et al., 2007; Lenard and Berthoud, 2008).

While energy homeostasis refers to negative feedback mechanisms maintaining the body weight at set-points, the combination of both homeostatic and hedonic components of feeding leads to the establishment of feed-forward mechanisms of physiological adaptations. Feed-forward adaptation, also known as allostasis (stability through changes), is critical in shaping energy balance and metabolic efficiency (McEwen and Wingfield, 2003) but also in contributing to reward-associated events (George et al., 2012; Keramati and Gutkin, 2014). Indeed, the facilitated access to and the widespread consumption of palatable diets have profoundly altered the delicate allostatic integration of homeostatic and hedonic signals, thereby leading to the development of metabolic disorders. This is particularly evident in food reward-driven dysfunctions such as binge eating (BE), where the uncontrolled feeding perfectly recapitulates the efforts for an organism to adapt its homeostatic processes to the hedonic aspects of feeding. In fact, short- and/or long-term consumption of energy-rich palatable diets promotes dopamine (DA) release from the ventral tegmental area (VTA) of the reward system (Rada et al., 2005; Small et al., 2003; Wise, 2004) as well as functional adaptations within the hypothalamus (Beutler et al., 2020; Linehan et al., 2020; Mazier et al., 2019; Rossi et al., 2019; Wei et al., 2015). Integrative allostatic mechanisms in the hypothalamus

and reward systems play a major role in ensuring metabolic efficiency and adaptation. Beyond these two core processors of feeding, recent reports have mechanistically demonstrated that the gut-brain vagal axis, beside sensing interoceptive signals and influencing feeding and energy homeostasis (Bai et al., 2019; Kaelberer et al., 2018; de Lartigue, 2016), is also a major modulator of the reward system (Fernandes et al., 2020; Han et al., 2016, 2018; Hankir et al., 2017; Malbert et al., 2019; Tellez et al., 2013). However, the physiological processes by which the gut-to-brain axis modulates reward feeding remain still unclear. Emerging evidence strongly suggests that, besides a plethora of peripheral hormones (i.e. ghrelin, leptin, GLP-1, CCK) (Gribble and Reimann, 2019), peripheral endocannabinoids (eCBs) may be fundamental players in the regulation of feeding and metabolic efficiency (Argueta and DiPatrizio, 2017; Capasso et al., 2018; DiPatrizio et al., 2013; Gómez et al., 2002; Izzo et al., 2009). Indeed, eating disorders-associated alterations in peripheral eCBs have been reported in obese and BE patients (Monteleone et al., 2016, 2017, 2005; Quarta et al., 2011) as well as in diet-induced obese rodents (Argueta and DiPatrizio, 2017; Kuipers et al., 2018). However, whether and how peripheral eCBs play a permissive role in both guiding reward-based feeding behaviors and buffering the allostatic regulation of energy balance remain still unexplored.

To tackle this question, we took advantage of a physiologically relevant binge eating-like mouse paradigm which, by promoting anticipatory and escalated consummatory food responses, triggers reward-driven behavioral, molecular and homeostatic adaptations. Binge eating, which elicited DA-dependent molecular modifications in the dopaminoceptive and reward-related structures, the dorsal striatum (DS) and the nucleus accumbens (NAc), revealed a yet unappreciated integrative gut-to-brain orchestration requiring the modulatory actions of peripheral eCBs. In particular, we show that binge eating requires an orchestrated dialog between peripheral eCBs and both central hypothalamic and VTA structures through the gut-brain vagal axis, thus modulating both energy balance and reward-like events.

Material and methods

Animals

All experiments using animals were approved by the Animal Care Committee of the Université de Paris (CEB-25–2016). 8-10 weeks old male C57Bl/6J mice (20-30 grams, Janvier, Le Genest St Isle, France) were single-housed one week prior to any experimentation in a room maintained at 22 +/-1 °C, with light period from 7 AM to 7 PM. Regular chow diet (3 438 kcal/kg, protein 19%, fat 5%, carbohydrates 55%, of total kcal, reference #U8959 version 63 Safe, Augy, France) and water were provided *ad libitum*. *Drd2*-Cre mice (STOCK Tg(Drd2-cre) ER44Gsat/Mmucd, Jackson laboratory) were used for *in vivo* fiber photometry Ca^{2+} imaging in the VTA.

Behaviors

Palatable binge eating-like paradigm. Intermittent daily access to the palatable mixture (Intralipid 20% w/v + sucrose 10% w/v) was provided for 1 hour during 12-14 consecutive days at 10-11 AM in home cages. During time-locked binge sessions regular chow pellets were not removed. Volume (mL) of consumed palatable mixture was measured at the end of the session.

Locomotor activity. Locomotor activity (LMA) was measured in an automated online measurement system using an infrared beam-based activity monitoring system (Phenomaster, TSE Systems GmbH, Bad Homburg, Germany).

Tail suspension. To record the activity GCaMP6f-expressing VTA neurons, mice were suspended above the ground by their tails. Ca^{2+} imaging was performed before and after tail suspension.

Exploratory drive in a new environment. To record the activity GCaMP6f-expressing VTA neurons in a novelty-induced exploratory drive, mice were put in a new cage (NC). Ca^{2+} imaging acquisition and analysis were performed before and after changing the environment.

HFHS-induced increased VTA activity. Animals were provided with a high-fat high-sugar pellet to validate the recording of VTA DA-neurons (activation) in *Drd2*-Cre mice. Ca^{2+} imaging acquisition and analysis were performed before and after feeding.

Scruff restraint. Animals were immobilized by restraining to validate the recording of VTA DA-neurons (inhibition) in *Drd2*-Cre mice. Ca^{2+} imaging acquisition and analysis were performed before and after scruff restraint.

Metabolic efficiency analysis

Mice were monitored for whole energy expenditure (EE) or Heat (H), O_2 consumption and CO_2 production, respiratory exchange rate ($RER=VCO_2/VO_2$, where V is a volume), and locomotor activity using calorimetric cages with bedding, food and water (Labmaster, TSE Systems GmbH, Bad Homburg, Germany). Ratio of gases was determined through an indirect open circuit calorimeter [for review (Arch et al., 2006; Even and Nadkarni, 2012)]. This system monitors O_2 and CO_2 concentration by volume at the inlet ports of a tide cage through which a known flow of air is being ventilated (0.4 L/min) and compared regularly to a reference empty cage. For optimum analysis, the flow rate was adjusted according to the animal body weights to set the differential in the composition of the expired gases between 0.4 and 0.9% (Labmaster, TSE Systems GmbH, Bad Homburg, Germany). The flow was previously calibrated with O_2 and CO_2 mixture of known concentrations (Air Liquide, S.A. France). Oxygen consumption and carbon dioxide production were recorded every 15 min for each animal during the entire experiment. Whole energy expenditure (EE) was calculated using the Weir equation for respiratory gas exchange measurements. Food consumption was measured as the instrument combines a set of highly sensitive feeding sensors for automated online measurements. Mice had access to food and water *ad libitum*. To allow measurement of every ambulatory movement, each cage was embedded in a frame with an infrared light beam-based activity monitoring system with online measurement at 100 Hz. The sensors for gases and detection of movements operated efficiently in both light and dark phases, allowing continuous recording.

Mice were monitored for body weight and composition at the entry and the exit of the experiment. Body mass composition (lean tissue mass, fat mass, free water and total water content) was analyzed using an Echo Medical systems' EchoMRI (Whole Body Composition Analyzers, EchoMRI, Houston, USA), according to manufacturer's instructions. Briefly, mice were weighed before they were put in a mouse holder and inserted in the MRI analyzer. Readings of body composition were given within 1 min.

Data analysis was performed on Excel XP using extracted raw values of VO_2 consumed, VCO_2 production (expressed in ml/h), and energy expenditure (kcal/h).

Triglycerides, insulin and corticosterone measurements

Plasma circulating triglycerides (TG) were measured with a quantitative enzymatic measurement (Serum Triglyceride Determination Kit, Sigma-Aldrich, Saint-Louis, USA). Insulin dosage was performed with ELISA kit (mouse ultrasensitive insulin ELISA, ALPCO, Salem, NH, USA). Corticosterone was measured with RIA kit (MP Biomedicals, Orangeburg, NY, USA). All kits were used according to the manufacturer guidelines.

Brown adipose tissue and telemetry body temperature measurements

Infrared camera for BAT temperature: heat production was visualized using a high-resolution infrared camera (FLIR E8; FLIR Systems, Portland, OR, USA). To measure brown adipose tissue (BAT) temperature, images of interscapular regions were captured before and after binge sessions. Infrared thermography images were analyzed using the FLIR TOOLS.

Telemetry body temperature: telemetric devices (Data Sciences International, accuracy 0.1°C) were implanted according to the manufacturer instructions. Briefly, single-housed mice were anesthetized with isoflurane (1-2%) and received ip injection of 10 mg/kg buprenorphine (Buprecare® 0.3 mg/ml) and 10 mg/kg ketoprofen (Ketofen® 10%). The transmitter (HD-XG; Data Sciences International) was placed intraperitoneally to measure longitudinal fluctuations of the core temperature. After surgery, animals were allowed to recover at 35°C and received a daily ip injection of ketoprofen (Ketofen® 10%) for 3 consecutive days. During a 7-day recovery period, mice were carefully monitored for body weight and behavior and had facilitated access to food. Implanted animals were then installed on their own receiver. Data were collected using the Ponemah® software (DSI). The detection of the transmitter signals was accomplished by a radio receiver (body temperature and locomotor activity) and processed by a microcomputer system.

Oral glucose tolerance test (OGTT)

Oral glucose tolerance test was performed following the establishment of binge-like behavior. Animals were fasted 6 hours before oral gavage of glucose (2 g/kg). Blood

glucose was directly measured from the vein blood tail using a glucometer (Menarini, Diagnotics, Rungis, France) at 0, 15, 30, 45, 60, 90, and 120 min. Blood samples were taken at 0, 15 and 30 and 60 min to measure insulin levels. Insulin dosage was performed with ELISA kit (mouse ultrasensitive insulin ELISA (ALPCO, Salem, NH, USA), according to the manufacturer guidelines).

Tissue preparation and immunofluorescence

For immunohistochemistry, animals were injected with i.p. pentobarbital (500 mg/kg, i.p., Sanofi-Aventis, France). Once anaesthetized, animals were transcardially perfused with 4°C PFA 4% for 5 minutes. Brains were collected, put overnight in PFA 4% and then stored in PBS, 4°C. 30 µm-thick sections were sliced with a vibratome (Leica VT1000S, France), and stored in PBS 4°C. Sections were processed as follows: Day 1: free-floating sections were rinsed in Tris-buffered saline (TBS; 0.25 M Tris and 0.5 M NaCl, pH 7.5), incubated for 5 min in TBS containing 3% H2O2 and 10% methanol, and then rinsed three times for 10 min each in TBS. After 15 min incubation in 0.2% Triton X-100 in TBS, sections were rinsed three times in TBS again. Slices were then incubated overnight or 48 hrs at 4°C with the following primary antibodies: rabbit anti-phospho-rpS6 $Ser^{235/236}$ (1:1000, Cell Signaling Technology, #2211), rabbit anti-phospho-rpS6 $Ser^{240/244}$ (1:1000, Cell Signaling Technology, #2215), rabbit anti-cFos (1:1000, Synaptic Systems, #226 003) or mouse anti-TH (1:1000, Millipore, #MAB318). Sections were rinsed three times for 10 min in TBS and incubated for 60 min with second anti-rabbit Cy3 AffiniPure (1:1000, Jackson Immunoresearch). Sections were rinsed for 10 min twice in TBS and once in TB (0.25 M Tris) before mounting.

Acquisitions were performed with a confocal microscope (Zeiss LSM 510). Images used for quantification were all single confocal sections. The objectives and the pinhole setting remained unchanged during the acquisition of a series for all images. Quantification of immunoreactive cells was performed using the cell counter plugin of the ImageJ software taking as standard reference a fixed threshold of fluorescence.

Western blotting

At the end of the binge session, the mouse head was cut and immediately immersed in liquid nitrogen for 3 seconds. The brain was then removed and dissected on ice-cold surface, sonicated in 200 µl (dorsal striatum) and 100 µl (nucleus accumbens) of

1% SDS supplemented with 0.2% phosphatase inhibitors and 1% protease inhibitors, and boiled for 10 minutes. Aliquots (2.5 µl) of the homogenates were used for protein quantification using a BCA kit (BC Assay Protein Quantitation Kit, Interchim Uptima, Montluçon, France). Equal amounts of proteins (10 µg) supplemented with a Laemmli buffer were loaded onto 10% polyacrylamide gels. Proteins were separated by SDS-PAGE and transferred to PVDF membranes (Millipore). The membranes were immunoblotted with the following antibodies: rabbit anti-phospho-Ser$^{235/236}$-rpS6 (1:1000, Cell Signaling Technology, #2211), rabbit anti-phospho-Ser$^{240/244}$-rpS6 (1:1000, Cell Signaling Technology, #2215), rabbit anti-phospho-ERK (1:2000, Cell Signaling Technology, #4370), mouse anti-beta-actin (1:5000, Sigma Aldrich, #A1978). Detection was based on HRP-coupled secondary antibody binding using ECL. The secondary antibodies were anti-mouse (1:5000, Dako, #P0260) and anti-rabbit (1:10000, Cell Signaling Technology, #7074). Membranes were imaged using the Amersham Images 680. Quantifications were performed using the ImageJ software.

Drug treatments

The following compounds were used: insulin (0.5 U/kg, Novo Nordisk, Lot GT67422), CCK-8S (10 ug/kg, Tocris, #1166), liraglutide (100 ug/kg, gift from Novo Nordisk), exendin 4 (10 ug/kg, Tocris, #1933), leptin (0.25 mg/kg, Tocris, #2985), AM251 (3 mg/kg, Tocris, #1117), AM6545 (10 mg/kg, Tocris, #5443), SKF81297 (5 mg/kg, Tocris, #1447), haloperidol (0.25 and 0.5 mg/kg, Tocris, #0931), SCH23390 (0.1 mg/kg, Tocris, #0925), GBR12909 (10 mg/kg, Sigma Aldrich, #D052), d-amphetamine sulphate (2 mg/kg, Tocris, #2813), JZL184 (8 mg/kg, Tocris, #3836).

Subdiaphragmatic vagotomy

Prior to surgery and during 3 post-surgery days, animals were provided with *ad libitum* jelly food (DietGel Boost Clear H_2O) to avoid the presence of solid food in the gastrointestinal tract. Animals received Buprécare® (Buprenorphine 0.3 mg) diluted 1/100 in NaCl 0.9% and Ketofen® (Ketoprofen 100 mg) diluted 1/100 in NaCl 0.9% and were anaesthetized with 3.5% isoflurane for induction and 1.5% for maintenance during the surgery. Their body temperature was maintained at 37°C. Briefly, using a binocular microscope, the right and left vagus nerve branches were carefully isolated along the esophagus and sectioned in vagotomized animals or left intact in sham

281 animals. Mice spent at least 3 weeks of post-surgery recovery period before being
282 used for the experimental procedures.
283
284 **Quantification of plasma eCBs**
285 Blood was collected before and after the last binge session and immediately
286 centrifuged to isolate the plasma. Plasma (50 µL) was added to vials containing
287 dichloromethane (8 mL), methanol (MeOH, 4 mL) (containing BHT), water
288 (containing EDTA) and the internal standards (deuterated *N*-acylethanolamines,
289 deuterated 2-AG). Following extraction, the lipid-containing fraction was purified by
290 solid phase extraction (SPE). The endocannabinoids and related NAEs were
291 recovered from the SPE column using hexane-isopropanol 7:3 (v/v) and transferred
292 to injection vials (Bottemanne et al., 2019). The samples (1 µL) were analyzed using
293 an Acquity UPLC® class H coupled to a Xevo TQ-S mass spectrometer (both from
294 Waters). For the separation we used an Acquity UPLC® BEH C18 (2.1x50 mm; 1.7
295 µm, 40°C) column and a gradient (200 µL/min) between MeOH-H_2O-acetic acid
296 (75:24.9:0.1; v/v/v) and MeOH-acetic acid (99.9:0.1; v/v). Ionization was obtained
297 using an ESI source operated in the positive mode. A quantification and a
298 qualification transition were optimized for each analyte and MassLynx® used for data
299 acquisition and processing. For each analyte, the ratio between the AUC of the lipid
300 and the AUC of the corresponding internal standard was used for data normalization.
301 Calibration curves were obtained in the same conditions.
302
303 **Viral production**
304 pAAV.Syn.Flex.GCaMP6f.WPRE.SV40 (titer ≥ 1×10^{13} vg/ml, working dilution 1:5)
305 was a gift from Douglas Kim (Addgene viral prep #100833-AAV9;
306 https://www.addgene.org/100833/; RRID:Addgene_100833).
307
308 **Stereotaxic procedure**
309 Mice were anaesthetized with isoflurane and received 10 mg/kg intraperitoneal
310 injection (i.p.) of Buprécare® (Buprenorphine 0.3 mg) diluted 1/100 in NaCl 0.9% and
311 10 mg/kg of Ketofen® (Ketoprofen 100 mg) diluted 1/100 in NaCl 0.9%, and placed
312 on a stereotactic frame (Model 940, David Kopf Instruments, California).
313 pAAV.Syn.Flex.GCaMP6f.WPRE.SV40 (0.3 µl) was injected unilaterally (for fiber
314 photometry) into the ventral tegmental area (VTA) (L=−0.5; AP=−3.4; V=−4.4, mm) of

Drd2-Cre mice at a rate of 0.05 µl/min. The injection needle was carefully removed after 5 minutes waiting at the injection site and 2 minutes waiting halfway to the top. Optical fiber for calcium imaging into the VTA was implanted 100 µm above the viral injection site. Animals were tested 4 weeks after viral stereotaxic injections.

Fiber photometry and data analysis

A chronically implantable cannula (Doric Lenses, Québec, Canada) composed of a bare optical fiber (400 µm core, 0.48 N.A.) and a fiber ferrule was implanted 100 µm above the location of the viral injection site in the ventral tegmental area (VTA: L=+/−0.5; AP=−3.4; V=−4.4, mm). The fiber was fixed onto the skull using dental cement (Super-Bond C&B, Sun Medical). Real-time fluorescence signals emitted from the calcium indicator GCaMP6f expressed by D2R-containing VTA neurons were recorded and analyzed as previously described (Lerner et al., 2015). Fluorescence was collected in the VTA using a single optical fiber for both delivery of excitation light streams and collection of emitted fluorescence.

The fiber photometry setup used 2 light-emitting LEDs: 405 nm LED sinusoidally modulated at 330 Hz and a 465 nm LED sinusoidally modulated at 533 Hz (Doric Lenses) merged in a FMC4 MiniCube (Doric Lenses) that combines the 2 wavelengths excitation light streams and separate them from the emission light. The MiniCube was connected to a Fiberoptic rotary joint (Doric Lenses) connected to the cannula. A RZ5P lock-in digital processor controlled by the Synapse software (Tucker-Davis Technologies, TDT, USA), commanded the voltage signal sent to the emitting LEDs via the LED driver (Doric Lenses). The light power before entering the implanted cannula was measured with a power meter (PM100USB, Thorlabs) before the beginning of each recording session. The irradiance was ~9 mW/cm^2. GCaMP6f-emitted fluorescence was collected by a femtowatt photoreceiver module (Doric Lenses) through the same fiber patch cord. The signal was then received by the RZ5P processor (TDT). On-line real-time demodulation of the fluorescence due to the 405nm and the 465 nm excitations was performed by the Synapse software (TDT). A camera was synchronized with the recording using the Synapse software.

Signals were exported to Python 3.0 and analyzed off-line using TDT Python SDK packages.

For the new cage paradigm, signal analysis was performed on two-time intervals: one extending from −60 to 0 seconds (home cage, HC) and the other from 0 to 60 seconds (new cage, NC).

For the tail suspension paradigm, signal analysis was performed on two-time intervals: one extending from −60 to 0 seconds (baseline) and the other from 0 to 120 seconds (tail suspension).

ΔF/F was calculated as [(465 nm $signal_{test}$ − fitted 405 nm $signal_{ref}$)/fitted 405 nm $signal_{ref}$]. To compare signal variations between the two conditions (NC *vs* HC or tail suspension *vs* baseline) for each mouse a difference between AUCs (AUC_2-AUC_1) was used.

Statistics

Data are presented as mean ± SEM. All statistical tests were performed with Prism 6 (GraphPad Software, La Jolla, CA, USA). The detailed statistical analyses are listed in the Supplementary Table 1. Depending on the experimental design, data were analyzed using either Student t-test (paired or unpaired) with equal variances, One-way ANOVA or Two-way ANOVA. In all cases, the significance threshold was automatically set at $p < 0.05$. ANOVA analyses were followed by Bonferroni *post hoc* test for specific comparisons only when overall ANOVA revealed a significant difference (at least $p < 0.05$).

Results

Time-locked access to palatable diet induces adaptation of nutrient partitioning and metabolic efficiency

Several preclinical paradigms of bingeing are widely used to model humans' eating disorders (Avena, 2010). However, the majority of currently available paradigms mainly rely on (*i*) prior alterations of basal homeostasis (food or water restriction/deprivation, stress induction), (*ii*) dietary exposure to either high-sugar or high-fat foods or (*iii*) the absence of food choice during bingeing periods.

We therefore adapted existing protocols to better study reward and homeostatic components of food intake during binge eating (BE). In our protocol, since dietary mixtures of fat and sugar lead to enhanced food reward properties (DiFeliceantonio et al., 2018), a highly palatable milkshake (sugar and fat) was designed to promote intense craving and reward-driven feeding. Time-locked access to this milkshake was sufficient to drive escalating binge-like consumption with no need of restricting access to chow diet (**Figure 1A**). In that regard, we are confident that our BE model is preferentially driven by reward values over metabolic demands since animals are neither food nor water restricted.

Mice intermittently exposed to this dietary palatable mixture rapidly maximized their intake within a few days, reaching an averaged consumption of 1.4 mL in 1h (~3.4 kcal/h) (**Figure 1B**). Importantly, intermittent (1h/day) exposure to palatable non-caloric sucralose or saccharin solutions did not lead to escalating binge-like consumption (**Suppl. Figure 1A, B**), indicating that calorie content, beyond taste perception itself, is necessary to drive incentive salience and BE-like behavior.

This palatable food consumption was simultaneously associated with an increased anticipatory locomotor activity ~2 hours before food access and lasted for another ~1-2 hours following access (**Figure 1C, C[1]**), with no changes in the ambulatory activity during the dark phase (**Figure 1C**). The same animals were characterized by a significant reduction in spontaneous nocturnal food intake (**Figure 1D, D[1]**). However, in bingeing animals the overall calories intake [standard diet (SD) + palatable food (PF)] remained identical to controls, thus indicating a conserved isocaloric maintenance in calories consumption despite reward-driven food intake (**Figure 1E**). Importantly, isocaloric feeding was associated with conserved body weight (BW) and body composition during the experimental protocol (**Figure 1F,**

Suppl. Figure 1C, D). Next, we investigated the consequence of palatable food exposure and BE progression onto metabolic efficiency. Indirect calorimetry analysis revealed an increase in the respiratory exchange ratio (RER) before and after intermittent palatable food consumption (**Figure 1G, G[1]**), and a stark reduction was detected in the dark phase (**Figure 1G**), thereby highlighting a metabolic shift of energy substrates use (from carbohydrates to lipids as indicated by RER ~1 or RER ~0.7 respectively). Such metabolic shift toward lipid substrates was further confirmed by the modulation of fatty acids oxidation (FAO, **Suppl. Figure 1E**). In addition, we also observed an increase in energy expenditure (EE) during the food anticipatory and consummatory phases (**Figure 1H, H[1]**). Furthermore, infrared thermography analysis revealed that BE was associated with a transient increase in brown adipose tissue (BAT) energy dissipation (**Figure 1I**) while telemetric recording of core body temperature revealed a BE specific increase during the anticipatory, consummatory and post-prandial phases (**Figure 1J, J[1], Suppl. Figue 1F**) and a sharp reduction during the last hours of the dark phase in BE animals. Overall, changes in core body temperature were fostered around the time of time-locked palatable food access and overlapped with the increase in locomotor activity (**Figure 1J, K**).

Access to calories-rich food and time-restricted feeding are invariably associated with changes in circulating signals reflecting metabolic and behavioral adaptations (Oosterman et al., 2020). In line with this, we observed that our model of BE was associated with reduced circulating triglycerides (TG) and insulin and concomitant increase in circulating corticosterone during the anticipatory phase (**Figure 2A-C**) while overall insulin sensitivity, as assessed by oral glucose tolerance test, remained unchanged (**Figure 2D, E**). These data support the notion that homeostatic adaptations occurring during time-locked palatable feeding lead to changes in lipid-substrates utilization and promotes adaptive activation of the hypothalamic-pituitary-adrenal (HPA) axis.

Overall, these results point to a rapid allostatic adaptation of metabolic and behavioral readouts, during which animals optimize their palatable food consumption and physiologically adapt by compensating the time-locked calories load to maintain a stable body weight.

BE induces dopamine-related modifications in a D1R-dependent manner

Dopamine (DA) neurons and DA-sensitive structures, such as the dorsal striatum (DS) and the nucleus accumbens (NAc), are critical players in reward-based paradigms but also in BE disorders (Balodis et al., 2015; Palmiter, 2007; Spierling et al., 2020; Wang et al., 2011). Here, we investigated whether bingeing modulated the DA-associated signaling machinery. Thus, we used the activation (phosphorylation) of the ribosomal protein S6 (rpS6) and the extracellular signal-regulated kinases (ERK) as functional readouts of DA-dependent molecular activity (Gangarossa et al., 2013a, 2013b, 2019; Valjent et al., 2019). We first investigated such molecular activations in bingeing mice before and after reward-diet consumption (**Figure 3A**) in the DS and NAc (**Figure 3B**).

The food anticipatory phase was associated with an increase in ERK activation only in the DS (**Figure 3C, D**), mostly reflecting the increased locomotor activity during the anticipatory phase. Importantly, palatable food consumption induced an increase in phospho-ERK and phospho-rpS6 (at both $Ser^{235/236}$ and $Ser^{240/244}$ sites) in both DS and NAc (**Figure 3C-E**). Interestingly, acute (single) consumption of palatable diet failed in triggering ERK and rpS6 activation (**Figure 3C-E**), thus revealing that molecular adaptation of the DA signaling in the DS/NAc are tightly dependent on the full establishment of the binge behavior and not only on the consumption of the palatable food. Immunofluorescence analysis revealed that BE-induced rpS6 activation was clearly evident in the DS and NAc (**Figure 3F, G**).

Next, we wondered whether food-reward anticipatory and/or consummatory phases were followed by adaptive changes in DA-evoked behavioral responses. Thus, we treated mice with GBR12909 (10 mg/kg), a specific dopamine transporter (DAT) blocker that prevents the presynaptic reuptake of DA, ultimately leading to its accumulation into the synaptic cleft. Interestingly, we observed a different behavior depending on BE phases (anticipatory *vs* consummatory). Before palatable food access, GBR treatment increased locomotor activity in both bingeing and control animals (**Figure 4A, A^1**). However, when GBR was administered following palatable food consumption (1h), GBR-induced locomotor response was blunted in bingeing animals (**Figure 4B, B^1**). These results indicate that BE-induced physiological adaptations are characterized by the enabled ability for palatable food to impinge on DA release and action. At the postsynaptic level, DA acts onto medium spiny neurons (MSNs) which express either the dopamine D1R (D1R-MSNs) or D2R (D2R-MSNs). In order to discriminate the role of D1R *vs* D2R signaling in BE, we

pretreated animals with the D1R antagonist SCH23390 (0.1 mg/kg) or vehicle (Veh) before providing access to palatable diet. SCH23390 dramatically reduced palatable food consumption (**Figure 4C**). On the contrary, pretreatment with haloperidol (0.25 and 0.5 mg/kg) did not dampen palatable food consumption (**Figure 4D**), even at doses (0.5 mg/kg) known to trigger cataleptic responses (Kobayashi et al., 1997; Radl et al., 2018). This evidence suggests that loss of control on palatable bingeing primarily relies on D1R signaling. In line with this event, activation of striatal D1R leads to downstream phosphorylation of rpS6 and ERK (Biever et al., 2015; Gangarossa et al., 2013a). Importantly, the adaptive molecular changes in the DS and NAc also required D1R activation since SCH23990 (0.1 mg/kg) largely suppressed BE-associated phosphorylations of rpS6 in both DS (**Figure 4E**) and NAc (**Figure 4F**). These results indicate that D1R is critical in driving palatable food consumption and its associated molecular activations in the specific context of BE. Of note, although SCH23390 reduced anticipatory locomotor activity in pretreated animals, basal locomotor activity in naive animals was not impaired (**Figure 4G, G^{1}**), thereby excluding the confounding effects due to changes in basal locomotor activity. Furthermore, a compensatory rescue in chow intake was observed in SCH23390-pretreated bingeing animals during the dark phase, excluding potential long-lasting effects of the D1R inhibition (**Figure 4H**). To further validate the hypothesis that D1R may be involved in BE-elicited dopamine modifications, we measured the locomotor activity triggered by the activation of D1R with its direct agonist SKF81297 (5 mg/kg) at the end of the BE session (1h after food access). At the end of the session, the D1R agonist SKF81297 (5 mg/kg) was administered to control and bingeing animals. Interestingly, we observed an earlier (first 30 min) significant increase in locomotor activity in bingeing animals compared to control mice (**Figure 4I, I^{1}**), although no major differences were detected during the cumulative 2-hrs response (**Figure 4I^{1}**). Overall, our results reveal that the critical phases surrounding palatable food consumption in the context of BE profoundly affect DA-associated signaling and promote consummatory and behavioral responses that primarily rely on D1R-dependent signaling.

Peripheral endocannabinoids govern binge eating

Recent studies have highlighted the role of enteric neuronal and endocrine systems in the regulation of food reward-seeking and DA-associated behaviors (de Araujo et

al., 2020; Reichelt et al., 2015). We therefore tested whether gut-born metabolic signals had a privileged action onto BE-like consumption of palatable diet when compared to other known circulating satiety signals.

Firstly, we observed that peripherally injected leptin (0.25 mg/kg), or insulin (0.5 U/kg), did not trigger any reduction in palatable food consumption when injected in bingeing animals (**Figure 5A**). Then, we investigated whether gut-born satiety signals retained anorectic properties with a similar protocol. Glucagon-like peptide hormone (GLP-1) is a satiety signal produced by the endocrine cells of the intestine. GLP-1R agonists, exendin-4 and liraglutide, are known to decrease food intake (Ladenheim, 2015). Both GLP-1 mimetic drugs (exendin-4, 10 µg/kg and liraglutide, 100 µg/kg) successfully reduced binge-consumption of palatable diet (**Figure 5A**). Similarly, the cholecystokinin (CCK) analog CCK-8S (10 µg/kg) acutely decreased palatable food intake (**Figure 5A**).

These results indicate that dietary-induced BE is associated with the resistance to the satiety action of leptin and insulin, while the anorectic action of gut-born signals remains unaltered.

Bioactive lipids, among which endocannabinoids (eCBs), are important signals to relay nutrients-induced adaptive responses in the gut-brain axis (DiPatrizio and Piomelli, 2015; Lau et al., 2017). Therefore, we explored the plasticity and functions of eCBs signaling in dietary-induced BE.

First, we pharmacologically inhibited the CB1R with the selective inverse agonist AM251 (3 mg/kg). Blockade of CB1R dramatically reduced BE-like consumption (**Figure 5A**). Next, we wondered whether bingeing was accompanied by alterations in circulating peripheral eCBs [anandamide (AEA) and 2-arachidonoylglycerol (2-AG)] and eCBs-related species [docosahexanoyl ethanolamide (DHEA), oleoylethanolamide (OEA)]. While circulating *N*-acylethanolamines (AEA, DHEA, OEA) remained unaffected, time-locked palatable feeding induced a significant increase in 2-AG immediately after food consumption (**Figure 5B**).

Since the CB1R is highly expressed in both peripheral and central nervous systems, we were eager to distinguish the respective contribution of central or peripheral of CB1R signaling in BE outputs. Thus, we used the peripherally restricted CB1R neutral antagonist AM6545 (10 mg/kg, i.p.), a compound unable to cross the blood brain barrier (Boon et al., 2014; Cluny et al., 2010; Tam et al., 2010). Pretreatment with AM6545 (10 mg/kg, 1h before palatable-food access) induced a

stark abolishment of BE consumption when administered acutely (**Figure 5C**). Conversely, the increase of circulating eCB achieved through the pharmacological inhibition (JZL184, 8 mg/kg) of the enzyme responsible of 2-AG hydrolysis, the monoacylglycerol lipase (MAGL) (Long et al., 2009), resulted in an increase of palatable food consumption that was fully prevented by AM6545 (**Figure 5C**). This bidirectional modulatory action of eCBs/CB1R onto BE did not show signs of desensitization and remained efficient throughout 4 days of daily pharmacological intervention (**Figure 5D**). In the same line, thermogenic and locomotor activity analyses revealed that pretreatment with AM6545 strongly dampened both the anticipatory and consummatory phases of BE (**Figure 5E, F**).

These results indicate that peripheral CB1R signaling is sufficient to control compulsive eating in BE.

We next explored how peripheral CB1R signaling modulates metabolic efficiency in the context of BE. Pretreatment with AM6545 (10 mg/kg, i.p.) significantly increased fatty acid oxidation (FAO) (**Figure 5G, G^{1}**). Importantly, this AM6545-induced increased FAO did not depend neither on reduced calorie intake (Binge session) or basal calorie contents (NoBinge session) (**Figure 5G^{2}**) nor on altered energy expenditure (EE) (**Suppl. Figure 2A**).

These results indicate that acute manipulation of peripheral, brain-excluded, eCB tone affects nutrient partitioning and promotes a shift towards whole body lipid-substrate utilization.

Importantly, we observed neither blunted palatable feeding responses (**Figure 5H**) nor increased FAO (**Figure 5I**) when AM6545 was orally (p.o.) administered. These results suggest that, in our behavioral model, CB1R-mediated homeostatic adaptations do not depend on the lumen-oriented apical CB1R expression in endothelial or enteroendocrine intestinal cells (Argueta et al., 2019; Sykaras et al., 2012) but rather on non-lumen-oriented CB1R. Recent reports have indicated that CB1R is also expressed in vagal afferent neurons (Burdyga et al., 2010; Egerod et al., 2018). To discriminate between all vagal afferents, we performed a meta-analysis on recent single-cell transcriptomic results (Bai et al., 2019) obtained through a path-specific viral strategy of gut segments (**Figure 5J**). This analysis revealed, that *Cnr1* (gene encoding for CB1R), but not *Cnr2*, was highly enriched in all segments of the gut-brain vagal axis (**Figure 5K, Suppl. Figure 2B, C**) and that, together with well-

known afferent markers (*Slc17a6*, *Scn10a*, *Htr3a*, *Cartpt*, *Grin1*, *Phox2b*), *Cnr1* may be considered as a constitutive marker of vagal sensory neurons.

The gut-brain vagal axis is required for eCBs-mediated effects

We have shown that gut-brain satiety signals and peripheral CB1R signaling retained full anorectic potency while circulating signals, leptin and insulin, failed to decrease feeding in our BE model (**Figure 5**). Given that peripheral eCBs can mediate their action in part through the vagus nerve (Bellocchio et al., 2013) this result strongly supports a critical implication for gut-born nervous inputs in the establishment/maintenance of BE-like behavior. Thus, we took advantage of subdiaphragmatic gut vagotomy (VGX) to investigate whether the eCBs-vagus axis was necessary/sufficient to mediate the anti-bingeing effects. In sham mice, injection of the peripherally restricted CB1R antagonist AM6545 led to a strong increase in cFos-expressing neurons in the nucleus tractus solitarius (NTS) and the area postrema (AP) while the signal was fully abolished in vagotomized mice (**Figure 6A, A^1, A^2**). In addition, we observed a vagus-dependent increase in cFos also in the NTS-projecting lateral parabrachial nucleus (lPBN) (**Figure 6A**), indicating that peripheral modulation of eCB action influences central brain pathways.

We also observed that the integrity of the vagus nerve was essential to mediate the anorectic action of AM6545 on BE behavior (**Figure 6B**). Importantly, although vagotomy (VGX) *per se* was associated with a decrease in time-locked hedonic feeding and consequent BE-derived compensatory homeostatic adaptations (**Suppl. Figure 3**), peripheral CB1R antagonist did not trigger an additive anorectic response (**Figure 6B**) in VGX mice compared to sham mice. Furthermore, vagotomy abolished the increase in FAO following AM6545 administration observed in sham mice (**Figure 6C, C^1**, **6D, D^1**). These results demonstrate that the gut-brain vagal communication routes feeding and the metabolic components associated with BE.

These vagus-dependent homeostatic adaptations promoted by peripheral blockade of CB1R prompted us to investigate whether AM6545 was able to alter the activity of brainstem-projecting central structures that control feeding. Indeed, AM6545 induced a strong vagus-dependent increase of cFos-neurons in the hypothalamic regions PVN and DMH (**Figure 6E, E^1, F, F^1**), thereby indicating that the metabolic adaptations induced by peripheral blockade of CB1R require a vagus-mediated NTS→PBN→hypothalamus circuit whose nodes' activation control feeding and

energy homeostasis (Cheng et al., 2020; D'Agostino et al., 2016; Grill and Hayes, 2012).

Peripheral CB1R signaling routed by the vagus nerve controls the activity of VTA dopamine neurons

Since palatable bingeing also strongly relies on central DA-dependent mechanisms (**Figure 3, 4**), we therefore explored the functional connection between peripheral eCBs and gut-to-brain vagal axis in the modulation of the reward DA system. Naive mice were pretreated with AM6545 (10 mg/kg, i.p.) or vehicle before being administered with the DAT blocker GBR12909 (10 mg/kg). Blockade of peripheral CB1R drastically reduced GBR-induced locomotor activity (**Figure 7A, A^1**) as well as GBR-triggered cFos induction in the striatum (**Figure 7B, B^1**). Interestingly, AM6545 failed in contrasting amphetamine-induced locomotor activity (**Figure 7C**), thereby suggesting that inhibition of peripheral CB1R may modulate the intrinsic activity of DA-neurons rather than altering evoked DA release events.

These results reveal that inhibition of peripheral CB1R, besides promoting satiety and FAO, may dampen reward-driven feeding also by concomitantly reducing DA-neurons activity and consequent activation of the dopaminoceptive structures.

To directly address this point, VGX mice were pretreated with AM6545 prior to receiving GBR12909. Remarkably, ablation of the vagus nerve prevented AM6545-induced blunting of GBR-elicited locomotor activity (**Figure 7D, D^1**). Moreover, this vagus-to-brain effect was further highlighted by the lack of action of AM6545 when orally administered (**Figure 7E, E^1**), as reported for palatable bingeing (**Figure 5H**). When AM6545 was primarily contained to the lumen and epithelial surface of the gut through oral administration, no effects on GBR-mediated hyperlocomotion were observed.

This result supports the notion that the modulatory action of peripheral eCB signaling onto the gut-brain axis in controlling reward BE is located outside of gut lumen.

Finally, to fully establish that peripheral inhibition of CB1R modulates the activity of dopamine VTA neurons, we performed cell type-specific *in vivo* Ca^{2+} imaging of DA-neurons in presence or absence of AM6545. We took advantage of the *Drd2*-Cre mouse line to express virally mediated GCaMP6f in VTA DA-neurons (**Figure 7F**) since they co-express the autoreceptor D2R (Anzalone et al., 2012; Usiello et al., 2000). Indeed, using this mouse line we were able to detect activation and inhibition

of VTA DA-neurons following rewarding (high-fat high-sugar pellet) or aversive (scruff restraint) events (**Suppl. Figure 4A, B**), respectively. To trigger the activity of DA-neurons independently from food- or drugs-associated stimuli, we used two paradigms that modulate DA-neurons activity: exposure to a new environment (Takeuchi et al., 2016) which promotes exploration and tail suspension (Kolata et al., 2018) (**Figure 7G**). Importantly, inhibition of peripheral CB1R (AM6545) led to a reduced activation of VTA DA-neurons in both paradigms (**Figure 7H, I**), thus revealing that peripheral CB1R lead to the abolishment of BE through the activation of satietogenic (**Figure 5, 6**) and the inhibition of reward circuits (**Figure 7**).

Discussion

A characteristic feature of feeding behavior is its key ability to dynamically adapt to sensory and environmental stimuli signaling food availability. Such adaptive strategy is even more pronounced when food is palatable and energy-dense. Indeed, the control of feeding strategies requires complex and highly interacting systems that can hardly be unequivocally attributed to single structures or circuits.

In our study, by using *in vivo* integrative approaches, we observed that, first, palatable time-locked feeding mobilizes both homeostatic and hedonic components of feeding through fast, but yet physiological, allostatic adaptations. Second, such allostatic adaptations require a concerted involvement of central DA (hedonic drive) and peripheral eCBs signaling (homeostatic and hedonic drive). Third, the permissive role of peripheral eCBs fully relies on the vagus nerve which, by a polysynaptic circuit, controls the activity of both satietogenic and reward (dopamine) structures. Fourth, our results point to peripheral CB1R neutral antagonists as promising therapeutic tools to counteract eating as well as reward-related disorders.

Overall, our study describes for the first time the fundamental role of eCB/vagal gut-brain transmission as a core component of binge eating and its behavioral, cellular and molecular adaptations.

Here, by investigating the pathways involved in hedonic feeding in absence of induced hunger or energy deprivation, we provide evidence that the hedonic drive to eat, as triggered by our intermittent time-locked model, promotes rapid homeostatic compensations leading to escalating consumption of palatable food and to allostatic adaptations of energy metabolism. As such, caloric demands are fulfilled and classical energy-mediated homeostatic signals (leptin, insulin) do not seem to spontaneously interfere, thus providing us the opportunity to study food intake-related integrative pathways with the abstraction of the homeostatic *vs* hedonic discrepancy. In line with clinical data (Carr and Grilo, 2020; Hutson et al., 2018), we observed that binge-like feeding in lean animals is not necessarily associated with overweight gain and does not lead to disrupted body weight homeostasis. On the contrary, through an allostatic feed-forward mechanism, mice rapidly adapt to palatable food availability by reducing their nocturnal feeding patterns in order to maximize time-locked (1h) hedonic feeding. Such adaptations, ranging from increased anticipatory feeding

phase to pre-feeding increased corticosterone levels and food intake maximization, all represent key hallmarks of the compulsive and emotional states of BE patients (Bake et al., 2014; Muñoz-Escobar et al., 2019; Naish et al., 2019). The anticipatory feeding phase was associated with decreased levels of plasma TG and insulin, whereas both anticipatory and consummatory phases were characterized by increased energy expenditure, core temperature and metabolic efficiency, thereby suggesting a metabolic shift of nutrients' use. This observation perfectly mirrors the allostatic theory, which stands on the fact that an organism anticipates and adapts to environmental changes while accordingly adjusting several physiological parameters to maintain stable physiological states (De Ridder et al., 2016; Ramsay and Woods, 2014). Allostatic mechanisms have classically been discussed in terms of stress-related regulatory events. However, the hedonic value of a stimulus (food, recreational drugs) can function as a feed-forward allostatic factor (George et al., 2012).

During time-locked palatable feeding, such allostatic adaptations (anticipation and consumption of palatable food) required intact DA signaling. In fact, analysis of key DA-activated downstream phospho-targets in the DS and NAc highlighted specific patterns of molecular activation. Notably, while the anticipatory phase was associated with an increase in ERK and rpS6$^{Ser235/236}$ phosphorylations, the consummatory phase was also accompanied by a robust increase in mTOR-mediated rpS6$^{Ser240/244}$ activation. Such signaling events, which did not depend on a single episode of palatable food intake, required the dopamine D1R as administration of SCH23390, but not of the D2R antagonist haloperidol, prevented binge-like behavior and its associated molecular modifications. This is of interest since, contrary to the well-known molecular insights of drugs of abuse which require the D1R (Bertran-Gonzalez et al., 2008; Gore and Zweifel, 2013; Kai et al., 2015; Luo et al., 2011; Sutton and Caron, 2015), food-related disorders have usually been predominantly associated with altered D2R signaling (Caravaggio et al., 2015; Kenny et al., 2013; Michaelides et al., 2012). These results reveal that binge eating, characterized by transients and sudden urges of hedonic drive, requires, at least in its early phases, a D1R-mediated transmission. This D1R-dependent mechanism is in line with the affinity and time-dependent dynamics of dopamine effects (Luo et al., 2011) as well as with the molecular action of released DA which, by binding to

Ga(olf)-coupled D1R, would trigger the activation of the aforementioned pathways, whether activation of the Gi-coupled D2R would lead to their inhibition (Beaulieu and Gainetdinov, 2011; Valjent et al., 2019). However, in clear opposition to psychostimulants, which directly act at central DA synapses, food and food-mediated behaviors impact DA transmission through a plethora of indirect and often peripherally born long-range acting mediators. In fact, the central regulation of feeding behavior, either in its homeostatic and/or hedonic components, tightly depends on the fine orchestration of peripheral humoral and neuronal signals. Notably, nutrients, as demonstrated by intragastric infusion of fat and sugar (Alhadeff et al., 2019; Han et al., 2016; Hankir et al., 2017; Tellez et al., 2016), or gut-born signals (Cone et al., 2014; Fulton et al., 2006; Jerlhag et al., 2007; Reddy et al., 2018), are sufficient to modulate DA release in reward-related structures. Here, we observed that gut-born signals such as CCK, GLP1 and endocannabinoids (eCBs) are essential in gating bingeing. In particular, we found that time-locked consumption of palatable food was associated with a rise in peripheral endogenous eCBs, notably 2-AG. Furthermore, inhibition of the 2-AG-degrading enzyme MAG lipase resulted in a potentiation of palatable food consumption. Thus, by taking advantage of a peripherally restricted CB1R antagonist (Tam et al., 2010), we observed that administration of AM6545 was able to fully abolish both anticipatory and consummatory phases of hedonic feeding as well as the potentiated feeding induced by the MAG lipase inhibitor. These effects agree with the literature showing that endogenous peripheral eCBs are highly and dynamically modulated in eating disorders, and act as powerful mediators of the gut-to-brain integration (Gómez et al., 2002).

Previous studies have shown that chronic administration of AM6545 promoted long-term maintenance of weight loss and reduction of dyslipidemia in obesity (Boon et al., 2014; Cluny et al., 2010; Tam et al., 2010). Here, we show that single, as well as repeated (4 days), administration of AM6545 potently inhibits binge eating without altering body weight. The anorectic effects of peripheral blockade of CB1R have been, at least in part, attributed to the property of CB1R antagonists to promote fatty acid oxidation (FAO). In agreement with these studies, we have observed that acute administration of AM6545 was able to dramatically increase FAO independently of food intake. However, here we also demonstrate that such effects require the vagus

nerve since subdiaphragmatic vagotomy prevents both AM6545-mediated bingeing blockade and FAO increase. The action of endogenous eCBs as well as of AM6545 on CB1R-expressing vagal afferents (Burdyga et al., 2010; Egerod et al., 2018) may explain our results. In fact, an increase in endogenous eCBs during palatable feeding, in virtue of the inhibitory Gi-coupled signaling of CB1R, would inhibit the vagus nerve thus delaying NTS-reaching satiety signals and promoting food intake. On the contrary, peripheral blockade of CB1R, especially when peripheral eCB levels are endogenously high (i.e. binge eating, bulimia, obesity), would lead to a prompt disinhibition and to the concomitant activation of satietogenic brain pathways (NTS→PBN→PVN). Interestingly, it is worth to mention that in a non-hedonic feeding paradigm the anorectic properties of AM6545 did not require the vagus nerve (Cluny et al., 2010) and that under fasting or lipoprivic conditions the systemic CB1R inverse agonist SR141716A (rimonabant) modulated feeding by the sympathetic nervous system (SNS) (Bellocchio et al., 2013). Another site of action for peripheral eCBs is represented by CB1R-expressing gut cells (Argueta et al., 2019; Godlewski et al., 2019). Interestingly, oral administration of a peripheral CB1R antagonist resulted in a reduction of alcohol intake via a ghrelin-dependent and vagus-mediated mechanism (Godlewski et al., 2019). However, in our reward-driven feeding model, oral administration of AM6545 failed in mediating its modifications on metabolic efficiency as well as in preventing bingeing behavior, thus suggesting that lumen-oriented apical CB1R may not be involved in our mechanism. Intriguingly, recent studies have uncovered that sensory neuropod cells in the gut (Bohórquez et al., 2014, 2015) can synaptically signal with the juxtaposed vagal afferents using, among other possible mediators (Glass et al., 2017; Haber et al., 2017), the fast-acting neurotransmitter glutamate (Kaelberer et al., 2018). Whether this specialized gut-to-nerve synapse also mobilizes eCBs, as it occurs at most central excitatory synapses, remains to be determined.

Overall, it would not be hazardous to suggest that peripheral eCBs may impact feeding patterns through different integrative mechanisms which, depending on the location of peripheral CB1R, may strongly modulate distinct functional outputs. Indeed, these results call for a need to use cell-type and tissue-type-specific strategies to selectively delete CB1R and/or eCBs-producing enzymes in distinct compartments of the gastrointestinal tract and in the neuronal gut-brain axis.

In order to anatomically provide an explanatory gut-to-brain circuit able to support the vagus-mediated action of AM6545, we found a stark increase of cFos, a marker of neuronal activity, in key brain regions of the satietogenic neuronal pathway. Importantly, we reveal that blockade of peripheral CB1R signaling resulted in a strong vagus-dependent activation of the NTS as well as of its downstream connected structures, notably the lPBN and the hypothalamic PVN. This segmented activation of the gut→brainstem→hypothalamus path is most likely responsible for the AM6545-induced effects on bingeing and energy homeostasis since structure-specific activation of these nodes has been shown to reduce food intake and alter energy homeostasis (An et al., 2020; Campos et al., 2016; Carter et al., 2013; D'Agostino et al., 2016; Li et al., 2019a, 2019b; Roman et al., 2016). In addition to this satietogenic path and given the strong reward component of our time-locked feeding paradigm, we also uncover that AM6545-mediated vagus activation results in a dampened activation of VTA DA-neurons. In fact, peripheral blockade of CB1R also resulted in a stark blunting of the DA-dependent GBR-evoked increased locomotor activity and DA-mediated cFos expression in the nucleus accumbens, a functional output that requires the intact vagal gut-brain axis. However, such effect did not depend on the releasing capabilities of DA neurons since AM6545 failed in altering amphetamine-evoked locomotor activity. In addition, taking advantage of virally mediated GCaMP6f-evoked *in vivo* Ca^{2+} imaging of putative VTA DA-neurons (Anzalone et al., 2012; Bello et al., 2011), here we demonstrate that peripheral blockade of CB1R clearly reduces both basal and evoked activity of DA-neurons, a feature resembling the effects of vagal nerve stimulation (Manta et al., 2013; Perez et al., 2014).

The VTA has a heterogeneous connectivity (Morales and Margolis, 2017) and a single and monosynaptic circuit responsible for the inhibition DA-neurons through the AM6545-activated vagus nerve cannot be selectively sorted out yet. However, several satiety-related structures in the brainstem, hindbrain and hypothalamus are known to project and modulate, directly or indirectly, VTA DA-neurons (Alhadeff et al., 2012; Boughter et al., 2019; Faget et al., 2016; Grill and Hayes, 2012; Han et al., 2018; Nieh et al., 2016; Wang et al., 2015). Among these circuits, the PBN→VTA relay is of particular interest since excitatory PBN neurons also largely contact VTA GABA-neurons (Beier et al., 2015; Faget et al., 2016) which in turn may drive the

inhibition of VTA DA-neurons and consequent dampening of motivated behaviors.

Here, we show that DA-dependent adaptations require orchestrated inputs among which peripheral endocannabinoids, through the vagus nerve, allostatically scale the homeostatic and hedonic components of feeding and act as mandatory gatekeepers for adaptive responses of the reward circuit. Indeed, the gut-brain axis is increasingly incriminated as a key player of the regulation of energy metabolism (Clemmensen et al., 2017), and we show for the first time that BE is under the control of the vagus-mediated peripheral inputs. Pointing the peripheral eCBs as permissive actors of this eating disorder certainly brings novelty in the clinical investigations aimed at identifying innovative and non-invasive therapeutic strategies. Importantly, this study further points the gut-brain axis as privileged target to modulate brain structures that are functionally responsible for processing integrative cognitive and reward.

In conclusion, while further studies are warrant to fully untangle the key enteric actors responsible for this phenomenon, our study identifies a novel integrative mechanism by which peripheral endocannabinoids through the vagal gut-brain axis gate allostatic feeding by controlling satiety and reward events, thus also paving the way to target peripheral elements for brain disorders.

Acknowledgments

We thank Chloé Morel, Rim Hassouna, Anne-Sophie Delbes, Daniela Herrera Moro and Raphaël Denis for technical advice and support. Adrien Paquot (BPBL/UCLouvain) is acknowledged for its help with eCB quantification. We thank Olja Kacanski for administrative support, Isabelle Le Parco, Ludovic Maingault, Angélique Dauvin, Aurélie Djemat, Florianne Michel, Magguy Boa and Daniel Quintas for animals' care and Sabria Allithi for genotyping. We acknowledge the technical platform Functional and Physiological Exploration platform (FPE) of the Université de Paris (BFA - UMR 8251) and the animal core facility Buffon of the Université de Paris/Institut Jacques Monod. This work was supported by the Fyssen Foundation, Nutricia Research Foundation, Allen Foundation Inc., Université de Paris and CNRS. CB and EM were supported by fellowships from the *Fondation pour la Recherche Médicale* (FRM).

Author Contributions

C.B. and G.G. conceived, designed, performed and analyzed most of the experiments. J.C. performed surgeries and behavioral experiments. E.M. helped with molecular studies. E.F. performed vagotomy. C.M. helped with fiber photometry experiments. G.G.M. analyzed endocannabinoids levels. S.L. provided scientific guidance and critical feedback. S.L. and G.G. secured funding. G.G. supervised the whole project, interpreted the data and wrote the manuscript with contribution from all coauthors.

Declaration of Interests

The authors declare no competing interests.

References

Alhadeff, A.L., Rupprecht, L.E., and Hayes, M.R. (2012). GLP-1 neurons in the nucleus of the solitary tract project directly to the ventral tegmental area and nucleus accumbens to control for food intake. Endocrinology *153*, 647–658.

Alhadeff, A.L., Goldstein, N., Park, O., Klima, M.L., Vargas, A., and Betley, J.N. (2019). Natural and Drug Rewards Engage Distinct Pathways that Converge on Coordinated Hypothalamic and Reward Circuits. Neuron *103*, 891-908.e6.

An, J.J., Kinney, C.E., Tan, J.-W., Liao, G.-Y., Kremer, E.J., and Xu, B. (2020). TrkB-expressing paraventricular hypothalamic neurons suppress appetite through multiple neurocircuits. Nat Commun *11*, 1729.

Anzalone, A., Lizardi-Ortiz, J.E., Ramos, M., De Mei, C., Hopf, F.W., Iaccarino, C., Halbout, B., Jacobsen, J., Kinoshita, C., Welter, M., et al. (2012). Dual control of dopamine synthesis and release by presynaptic and postsynaptic dopamine D2 receptors. J Neurosci *32*, 9023–9034.

de Araujo, I.E., Schatzker, M., and Small, D.M. (2020). Rethinking Food Reward. Annual Review of Psychology *71*, 139–164.

Arch, J.R.S., Hislop, D., Wang, S.J.Y., and Speakman, J.R. (2006). Some mathematical and technical issues in the measurement and interpretation of open-circuit indirect calorimetry in small animals. Int J Obes (Lond) *30*, 1322–1331.

Argueta, D.A., and DiPatrizio, N.V. (2017). Peripheral endocannabinoid signaling controls hyperphagia in western diet-induced obesity. Physiol Behav *171*, 32–39.

Argueta, D.A., Perez, P.A., Makriyannis, A., and DiPatrizio, N.V. (2019). Cannabinoid CB1 Receptors Inhibit Gut-Brain Satiation Signaling in Diet-Induced Obesity. Front Physiol *10*, 704.

Avena, N.M. (2010). The study of food addiction using animal models of binge eating. Appetite *55*, 734–737.

Bai, L., Mesgarzadeh, S., Ramesh, K.S., Huey, E.L., Liu, Y., Gray, L.A., Aitken, T.J., Chen, Y., Beutler, L.R., Ahn, J.S., et al. (2019). Genetic Identification of Vagal Sensory Neurons That Control Feeding. Cell *179*, 1129-1143.e23.

Bake, T., Murphy, M., Morgan, D.G.A., and Mercer, J.G. (2014). Large, binge-type meals of high fat diet change feeding behaviour and entrain food anticipatory activity in mice. Appetite *77*, 60–71.

Balodis, I.M., Grilo, C.M., and Potenza, M.N. (2015). Neurobiological features of binge eating disorder. CNS Spectr *20*, 557–565.

Beaulieu, J.-M., and Gainetdinov, R.R. (2011). The physiology, signaling, and pharmacology of dopamine receptors. Pharmacol. Rev. *63*, 182–217.

Beier, K.T., Steinberg, E.E., DeLoach, K.E., Xie, S., Miyamichi, K., Schwarz, L., Gao, X.J., Kremer, E.J., Malenka, R.C., and Luo, L. (2015). Circuit Architecture of VTA Dopamine Neurons Revealed by Systematic Input-Output Mapping. Cell *162*, 622–634.

Bello, E.P., Mateo, Y., Gelman, D.M., Noaín, D., Shin, J.H., Low, M.J., Alvarez, V.A., Lovinger, D.M., and Rubinstein, M. (2011). Cocaine supersensitivity and enhanced motivation for reward in mice lacking dopamine D2 autoreceptors. Nat Neurosci *14*, 1033–1038.

Bellocchio, L., Soria-Gómez, E., Quarta, C., Metna-Laurent, M., Cardinal, P., Binder, E., Cannich, A., Delamarre, A., Häring, M., Martín-Fontecha, M., et al. (2013). Activation of the sympathetic nervous system mediates hypophagic and anxiety-like effects of CB_1 receptor blockade. Proc Natl Acad Sci U S A *110*, 4786–4791.

Berthoud, H.-R., Münzberg, H., and Morrison, C.D. (2017). Blaming the Brain for Obesity: Integration of Hedonic and Homeostatic Mechanisms. Gastroenterology

152, 1728–1738.

Bertran-Gonzalez, J., Bosch, C., Maroteaux, M., Matamales, M., Hervé, D., Valjent, E., and Girault, J.-A. (2008). Opposing patterns of signaling activation in dopamine D1 and D2 receptor-expressing striatal neurons in response to cocaine and haloperidol. J. Neurosci. *28*, 5671–5685.

Beutler, L.R., Corpuz, T.V., Ahn, J.S., Kosar, S., Song, W., Chen, Y., and Knight, Z.A. (2020). Obesity causes selective and long-lasting desensitization of AgRP neurons to dietary fat. Elife *9*.

Biever, A., Puighermanal, E., Nishi, A., David, A., Panciatici, C., Longueville, S., Xirodimas, D., Gangarossa, G., Meyuhas, O., Hervé, D., et al. (2015). PKA-dependent phosphorylation of ribosomal protein S6 does not correlate with translation efficiency in striatonigral and striatopallidal medium-sized spiny neurons. J. Neurosci. *35*, 4113–4130.

Bohórquez, D.V., Samsa, L.A., Roholt, A., Medicetty, S., Chandra, R., and Liddle, R.A. (2014). An enteroendocrine cell-enteric glia connection revealed by 3D electron microscopy. PLoS One *9*, e89881.

Bohórquez, D.V., Shahid, R.A., Erdmann, A., Kreger, A.M., Wang, Y., Calakos, N., Wang, F., and Liddle, R.A. (2015). Neuroepithelial circuit formed by innervation of sensory enteroendocrine cells. J Clin Invest *125*, 782–786.

Boon, M.R., Kooijman, S., van Dam, A.D., Pelgrom, L.R., Berbée, J.F.P., Visseren, C.A.R., van Aggele, R.C., van den Hoek, A.M., Sips, H.C.M., Lombès, M., et al. (2014). Peripheral cannabinoid 1 receptor blockade activates brown adipose tissue and diminishes dyslipidemia and obesity. FASEB J *28*, 5361–5375.

Bottemanne, P., Paquot, A., Ameraoui, H., Alhouayek, M., and Muccioli, G.G. (2019). The α/β-hydrolase domain 6 inhibitor WWL70 decreases endotoxin-induced lung inflammation in mice, potential contribution of 2-arachidonoylglycerol, and lysoglycerophospholipids. FASEB J *33*, 7635–7646.

Boughter, J.D., Lu, L., Saites, L.N., and Tokita, K. (2019). Sweet and bitter taste stimuli activate VTA projection neurons in the parabrachial nucleus. Brain Res *1714*, 99–110.

Burdyga, G., Varro, A., Dimaline, R., Thompson, D.G., and Dockray, G.J. (2010). Expression of cannabinoid CB1 receptors by vagal afferent neurons: kinetics and role in influencing neurochemical phenotype. Am J Physiol Gastrointest Liver Physiol *299*, G63-69.

Campos, C.A., Bowen, A.J., Schwartz, M.W., and Palmiter, R.D. (2016). Parabrachial CGRP Neurons Control Meal Termination. Cell Metab *23*, 811–820.

Capasso, A., Milano, W., and Cauli, O. (2018). Changes in the Peripheral Endocannabinoid System as a Risk Factor for the Development of Eating Disorders. Endocr Metab Immune Disord Drug Targets *18*, 325–332.

Caravaggio, F., Raitsin, S., Gerretsen, P., Nakajima, S., Wilson, A., and Graff-Guerrero, A. (2015). Ventral striatum binding of a dopamine D2/3 receptor agonist but not antagonist predicts normal body mass index. Biol Psychiatry *77*, 196–202.

Carr, M.M., and Grilo, C.M. (2020). Examining heterogeneity of binge-eating disorder using latent class analysis. J Psychiatr Res *130*, 194–200.

Carter, M.E., Soden, M.E., Zweifel, L.S., and Palmiter, R.D. (2013). Genetic identification of a neural circuit that suppresses appetite. Nature *503*, 111–114.

Cheng, W., Gonzalez, I., Pan, W., Tsang, A.H., Adams, J., Ndoka, E., Gordian, D., Khoury, B., Roelofs, K., Evers, S.S., et al. (2020). Calcitonin Receptor Neurons in the Mouse Nucleus Tractus Solitarius Control Energy Balance via the Non-aversive Suppression of Feeding. Cell Metab *31*, 301-312.e5.

960 Clemmensen, C., Müller, T.D., Woods, S.C., Berthoud, H.-R., Seeley, R.J., and
961 Tschöp, M.H. (2017). Gut-Brain Cross-Talk in Metabolic Control. Cell *168*, 758–774.
962 Cluny, N.L., Vemuri, V.K., Chambers, A.P., Limebeer, C.L., Bedard, H., Wood, J.T.,
963 Lutz, B., Zimmer, A., Parker, L.A., Makriyannis, A., et al. (2010). A novel peripherally
964 restricted cannabinoid receptor antagonist, AM6545, reduces food intake and body
965 weight, but does not cause malaise, in rodents. Br J Pharmacol *161*, 629–642.
966 Coll, A.P., Farooqi, I.S., and O'Rahilly, S. (2007). The hormonal control of food
967 intake. Cell *129*, 251–262.
968 Cone, J.J., McCutcheon, J.E., and Roitman, M.F. (2014). Ghrelin acts as an interface
969 between physiological state and phasic dopamine signaling. J Neurosci *34*, 4905–
970 4913.
971 D'Agostino, G., Lyons, D.J., Cristiano, C., Burke, L.K., Madara, J.C., Campbell, J.N.,
972 Garcia, A.P., Land, B.B., Lowell, B.B., Dileone, R.J., et al. (2016). Appetite controlled
973 by a cholecystokinin nucleus of the solitary tract to hypothalamus neurocircuit. Elife
974 *5*.
975 De Ridder, D., Manning, P., Leong, S.L., Ross, S., and Vanneste, S. (2016).
976 Allostasis in health and food addiction. Sci Rep *6*, 37126.
977 DiFeliceantonio, A.G., Coppin, G., Rigoux, L., Edwin Thanarajah, S., Dagher, A.,
978 Tittgemeyer, M., and Small, D.M. (2018). Supra-Additive Effects of Combining Fat
979 and Carbohydrate on Food Reward. Cell Metab *28*, 33-44.e3.
980 DiPatrizio, N.V., and Piomelli, D. (2015). Intestinal lipid-derived signals that sense
981 dietary fat. J Clin Invest *125*, 891–898.
982 DiPatrizio, N.V., Joslin, A., Jung, K.-M., and Piomelli, D. (2013). Endocannabinoid
983 signaling in the gut mediates preference for dietary unsaturated fats. FASEB J *27*,
984 2513–2520.
985 Egerod, K.L., Petersen, N., Timshel, P.N., Rekling, J.C., Wang, Y., Liu, Q., Schwartz,
986 T.W., and Gautron, L. (2018). Profiling of G protein-coupled receptors in vagal
987 afferents reveals novel gut-to-brain sensing mechanisms. Mol Metab *12*, 62–75.
988 Even, P.C., and Nadkarni, N.A. (2012). Indirect calorimetry in laboratory mice and
989 rats: principles, practical considerations, interpretation and perspectives. Am J
990 Physiol Regul Integr Comp Physiol *303*, R459-476.
991 Faget, L., Osakada, F., Duan, J., Ressler, R., Johnson, A.B., Proudfoot, J.A., Yoo,
992 J.H., Callaway, E.M., and Hnasko, T.S. (2016). Afferent Inputs to Neurotransmitter-
993 Defined Cell Types in the Ventral Tegmental Area. Cell Rep *15*, 2796–2808.
994 Fernandes, A.B., Alves da Silva, J., Almeida, J., Cui, G., Gerfen, C.R., Costa, R.M.,
995 and Oliveira-Maia, A.J. (2020). Postingestive Modulation of Food Seeking Depends
996 on Vagus-Mediated Dopamine Neuron Activity. Neuron *106*, 778-788.e6.
997 Fulton, S., Pissios, P., Manchon, R.P., Stiles, L., Frank, L., Pothos, E.N., Maratos-
998 Flier, E., and Flier, J.S. (2006). Leptin regulation of the mesoaccumbens dopamine
999 pathway. Neuron *51*, 811–822.
1000 Gangarossa, G., Perroy, J., and Valjent, E. (2013a). Combinatorial topography and
1001 cell-type specific regulation of the ERK pathway by dopaminergic agonists in the
1002 mouse striatum. Brain Struct Funct *218*, 405–419.
1003 Gangarossa, G., Espallergues, J., de Kerchove d'Exaerde, A., El Mestikawy, S.,
1004 Gerfen, C.R., Hervé, D., Girault, J.-A., and Valjent, E. (2013b). Distribution and
1005 compartmental organization of GABAergic medium-sized spiny neurons in the mouse
1006 nucleus accumbens. Front Neural Circuits *7*, 22.
1007 Gangarossa, G., Castell, L., Castro, L., Tarot, P., Veyrunes, F., Vincent, P., Bertaso,
1008 F., and Valjent, E. (2019). Contrasting patterns of ERK activation in the tail of the
1009 striatum in response to aversive and rewarding signals. J. Neurochem. *151*, 204–

226.
George, O., Le Moal, M., and Koob, G.F. (2012). Allostasis and addiction: role of the dopamine and corticotropin-releasing factor systems. Physiol Behav *106*, 58–64.
Glass, L.L., Calero-Nieto, F.J., Jawaid, W., Larraufie, P., Kay, R.G., Göttgens, B., Reimann, F., and Gribble, F.M. (2017). Single-cell RNA-sequencing reveals a distinct population of proglucagon-expressing cells specific to the mouse upper small intestine. Mol Metab *6*, 1296–1303.
Godlewski, G., Cinar, R., Coffey, N.J., Liu, J., Jourdan, T., Mukhopadhyay, B., Chedester, L., Liu, Z., Osei-Hyiaman, D., Iyer, M.R., et al. (2019). Targeting Peripheral CB1 Receptors Reduces Ethanol Intake via a Gut-Brain Axis. Cell Metab *29*, 1320-1333.e8.
Gómez, R., Navarro, M., Ferrer, B., Trigo, J.M., Bilbao, A., Del Arco, I., Cippitelli, A., Nava, F., Piomelli, D., and Rodríguez de Fonseca, F. (2002). A peripheral mechanism for CB1 cannabinoid receptor-dependent modulation of feeding. J Neurosci *22*, 9612–9617.
Gore, B.B., and Zweifel, L.S. (2013). Genetic reconstruction of dopamine D1 receptor signaling in the nucleus accumbens facilitates natural and drug reward responses. J Neurosci *33*, 8640–8649.
Gribble, F.M., and Reimann, F. (2019). Function and mechanisms of enteroendocrine cells and gut hormones in metabolism. Nat Rev Endocrinol *15*, 226–237.
Grill, H.J., and Hayes, M.R. (2012). Hindbrain neurons as an essential hub in the neuroanatomically distributed control of energy balance. Cell Metab *16*, 296–309.
Haber, A.L., Biton, M., Rogel, N., Herbst, R.H., Shekhar, K., Smillie, C., Burgin, G., Delorey, T.M., Howitt, M.R., Katz, Y., et al. (2017). A single-cell survey of the small intestinal epithelium. Nature *551*, 333–339.
Han, W., Tellez, L.A., Niu, J., Medina, S., Ferreira, T.L., Zhang, X., Su, J., Tong, J., Schwartz, G.J., van den Pol, A., et al. (2016). Striatal Dopamine Links Gastrointestinal Rerouting to Altered Sweet Appetite. Cell Metab *23*, 103–112.
Han, W., Tellez, L.A., Perkins, M.H., Perez, I.O., Qu, T., Ferreira, J., Ferreira, T.L., Quinn, D., Liu, Z.-W., Gao, X.-B., et al. (2018). A Neural Circuit for Gut-Induced Reward. Cell *175*, 665-678.e23.
Hankir, M.K., Seyfried, F., Hintschich, C.A., Diep, T.-A., Kleberg, K., Kranz, M., Deuther-Conrad, W., Tellez, L.A., Rullmann, M., Patt, M., et al. (2017). Gastric Bypass Surgery Recruits a Gut PPAR-α-Striatal D1R Pathway to Reduce Fat Appetite in Obese Rats. Cell Metab. *25*, 335–344.
Hutson, P.H., Balodis, I.M., and Potenza, M.N. (2018). Binge-eating disorder: Clinical and therapeutic advances. Pharmacol Ther *182*, 15–27.
Izzo, A.A., Piscitelli, F., Capasso, R., Aviello, G., Romano, B., Borrelli, F., Petrosino, S., and Di Marzo, V. (2009). Peripheral endocannabinoid dysregulation in obesity: relation to intestinal motility and energy processing induced by food deprivation and re-feeding. Br J Pharmacol *158*, 451–461.
Jerlhag, E., Egecioglu, E., Dickson, S.L., Douhan, A., Svensson, L., and Engel, J.A. (2007). Ghrelin administration into tegmental areas stimulates locomotor activity and increases extracellular concentration of dopamine in the nucleus accumbens. Addict Biol *12*, 6–16.
Kaelberer, M.M., Buchanan, K.L., Klein, M.E., Barth, B.B., Montoya, M.M., Shen, X., and Bohórquez, D.V. (2018). A gut-brain neural circuit for nutrient sensory transduction. Science *361*.
Kai, N., Nishizawa, K., Tsutsui, Y., Ueda, S., and Kobayashi, K. (2015). Differential roles of dopamine D1 and D2 receptor-containing neurons of the nucleus accumbens

shell in behavioral sensitization. J Neurochem *135*, 1232–1241.
Kenny, P.J., Voren, G., and Johnson, P.M. (2013). Dopamine D2 receptors and striatopallidal transmission in addiction and obesity. Curr Opin Neurobiol *23*, 535–538.
Keramati, M., and Gutkin, B. (2014). Homeostatic reinforcement learning for integrating reward collection and physiological stability. Elife *3*.
Kobayashi, T., Araki, T., Itoyama, Y., Takeshita, M., Ohta, T., and Oshima, Y. (1997). Effects of L-dopa and bromocriptine on haloperidol-induced motor deficits in mice. Life Sci *61*, 2529–2538.
Kolata, S.M., Nakao, K., Jeevakumar, V., Farmer-Alroth, E.L., Fujita, Y., Bartley, A.F., Jiang, S.Z., Rompala, G.R., Sorge, R.E., Jimenez, D.V., et al. (2018). Neuropsychiatric Phenotypes Produced by GABA Reduction in Mouse Cortex and Hippocampus. Neuropsychopharmacology *43*, 1445–1456.
Kuipers, E.N., Kantae, V., Maarse, B.C.E., van den Berg, S.M., van Eenige, R., Nahon, K.J., Reifel-Miller, A., Coskun, T., de Winther, M.P.J., Lutgens, E., et al. (2018). High Fat Diet Increases Circulating Endocannabinoids Accompanied by Increased Synthesis Enzymes in Adipose Tissue. Front Physiol *9*, 1913.
Ladenheim, E.E. (2015). Liraglutide and obesity: a review of the data so far. Drug Des Devel Ther *9*, 1867–1875.
de Lartigue, G. (2016). Role of the vagus nerve in the development and treatment of diet-induced obesity. J Physiol *594*, 5791–5815.
Lau, B.K., Cota, D., Cristino, L., and Borgland, S.L. (2017). Endocannabinoid modulation of homeostatic and non-homeostatic feeding circuits. Neuropharmacology *124*, 38–51.
Lenard, N.R., and Berthoud, H.-R. (2008). Central and peripheral regulation of food intake and physical activity: pathways and genes. Obesity (Silver Spring) *16 Suppl 3*, S11-22.
Lerner, T.N., Shilyansky, C., Davidson, T.J., Evans, K.E., Beier, K.T., Zalocusky, K.A., Crow, A.K., Malenka, R.C., Luo, L., Tomer, R., et al. (2015). Intact-Brain Analyses Reveal Distinct Information Carried by SNc Dopamine Subcircuits. Cell *162*, 635–647.
Li, C., Navarrete, J., Liang-Guallpa, J., Lu, C., Funderburk, S.C., Chang, R.B., Liberles, S.D., Olson, D.P., and Krashes, M.J. (2019a). Defined Paraventricular Hypothalamic Populations Exhibit Differential Responses to Food Contingent on Caloric State. Cell Metab *29*, 681-694.e5.
Li, M.M., Madara, J.C., Steger, J.S., Krashes, M.J., Balthasar, N., Campbell, J.N., Resch, J.M., Conley, N.J., Garfield, A.S., and Lowell, B.B. (2019b). The Paraventricular Hypothalamus Regulates Satiety and Prevents Obesity via Two Genetically Distinct Circuits. Neuron *102*, 653-667.e6.
Linehan, V., Fang, L.Z., Parsons, M.P., and Hirasawa, M. (2020). High-fat diet induces time-dependent synaptic plasticity of the lateral hypothalamus. Mol Metab *36*, 100977.
Long, J.Z., Li, W., Booker, L., Burston, J.J., Kinsey, S.G., Schlosburg, J.E., Pavón, F.J., Serrano, A.M., Selley, D.E., Parsons, L.H., et al. (2009). Selective blockade of 2-arachidonoylglycerol hydrolysis produces cannabinoid behavioral effects. Nat Chem Biol *5*, 37–44.
Luo, Z., Volkow, N.D., Heintz, N., Pan, Y., and Du, C. (2011). Acute cocaine induces fast activation of D1 receptor and progressive deactivation of D2 receptor striatal neurons: in vivo optical microprobe [Ca2+]i imaging. J Neurosci *31*, 13180–13190.
Lutter, M., and Nestler, E.J. (2009). Homeostatic and hedonic signals interact in the

regulation of food intake. J Nutr *139*, 629–632.
Malbert, C.-H., Genissel, M., Divoux, J.-L., and Henry, C. (2019). Chronic abdominal vagus stimulation increased brain metabolic connectivity, reduced striatal dopamine transporter and increased mid-brain serotonin transporter in obese miniature pigs. J Transl Med *17*, 78.
Manta, S., El Mansari, M., Debonnel, G., and Blier, P. (2013). Electrophysiological and neurochemical effects of long-term vagus nerve stimulation on the rat monoaminergic systems. Int J Neuropsychopharmacol *16*, 459–470.
Mazier, W., Saucisse, N., Simon, V., Cannich, A., Marsicano, G., Massa, F., and Cota, D. (2019). mTORC1 and CB1 receptor signaling regulate excitatory glutamatergic inputs onto the hypothalamic paraventricular nucleus in response to energy availability. Mol Metab *28*, 151–159.
McEwen, B.S., and Wingfield, J.C. (2003). The concept of allostasis in biology and biomedicine. Horm Behav *43*, 2–15.
Michaelides, M., Thanos, P.K., Kim, R., Cho, J., Ananth, M., Wang, G.-J., and Volkow, N.D. (2012). PET imaging predicts future body weight and cocaine preference. Neuroimage *59*, 1508–1513.
Monteleone, A.M., Di Marzo, V., Monteleone, P., Dalle Grave, R., Aveta, T., Ghoch, M.E., Piscitelli, F., Volpe, U., Calugi, S., and Maj, M. (2016). Responses of peripheral endocannabinoids and endocannabinoid-related compounds to hedonic eating in obesity. Eur J Nutr *55*, 1799–1805.
Monteleone, A.M., Piscitelli, F., Dalle Grave, R., El Ghoch, M., Di Marzo, V., Maj, M., and Monteleone, P. (2017). Peripheral Endocannabinoid Responses to Hedonic Eating in Binge-Eating Disorder. Nutrients *9*.
Monteleone, P., Matias, I., Martiadis, V., De Petrocellis, L., Maj, M., and Di Marzo, V. (2005). Blood levels of the endocannabinoid anandamide are increased in anorexia nervosa and in binge-eating disorder, but not in bulimia nervosa. Neuropsychopharmacology *30*, 1216–1221.
Morales, M., and Margolis, E.B. (2017). Ventral tegmental area: cellular heterogeneity, connectivity and behaviour. Nat Rev Neurosci *18*, 73–85.
Muñoz-Escobar, G., Guerrero-Vargas, N.N., and Escobar, C. (2019). Random access to palatable food stimulates similar addiction-like responses as a fixed schedule, but only a fixed schedule elicits anticipatory activation. Sci Rep *9*, 18223.
Naish, K.R., Laliberte, M., MacKillop, J., and Balodis, I.M. (2019). Systematic review of the effects of acute stress in binge eating disorder. Eur J Neurosci *50*, 2415–2429.
Nieh, E.H., Vander Weele, C.M., Matthews, G.A., Presbrey, K.N., Wichmann, R., Leppla, C.A., Izadmehr, E.M., and Tye, K.M. (2016). Inhibitory Input from the Lateral Hypothalamus to the Ventral Tegmental Area Disinhibits Dopamine Neurons and Promotes Behavioral Activation. Neuron *90*, 1286–1298.
Oosterman, J.E., Koekkoek, L.L., Foppen, E., Unmehopa, U.A., Eggels, L., Verheij, J., Fliers, E., la Fleur, S.E., and Kalsbeek, A. (2020). Synergistic Effect of Feeding Time and Diet on Hepatic Steatosis and Gene Expression in Male Wistar Rats. Obesity (Silver Spring) *28 Suppl 1*, S81–S92.
Palmiter, R.D. (2007). Is dopamine a physiologically relevant mediator of feeding behavior? Trends Neurosci *30*, 375–381.
Perez, S.M., Carreno, F.R., Frazer, A., and Lodge, D.J. (2014). Vagal nerve stimulation reverses aberrant dopamine system function in the methylazoxymethanol acetate rodent model of schizophrenia. J Neurosci *34*, 9261–9267.
Quarta, C., Mazza, R., Obici, S., Pasquali, R., and Pagotto, U. (2011). Energy balance regulation by endocannabinoids at central and peripheral levels. Trends Mol

Med *17*, 518–526.
Rada, P., Avena, N.M., and Hoebel, B.G. (2005). Daily bingeing on sugar repeatedly releases dopamine in the accumbens shell. Neuroscience *134*, 737–744.
Radl, D., Chiacchiaretta, M., Lewis, R.G., Brami-Cherrier, K., Arcuri, L., and Borrelli, E. (2018). Differential regulation of striatal motor behavior and related cellular responses by dopamine D2L and D2S isoforms. Proc Natl Acad Sci U S A *115*, 198–203.
Ramsay, D.S., and Woods, S.C. (2014). Clarifying the roles of homeostasis and allostasis in physiological regulation. Psychol Rev *121*, 225–247.
Reddy, I.A., Smith, N.K., Erreger, K., Ghose, D., Saunders, C., Foster, D.J., Turner, B., Poe, A., Albaugh, V.L., McGuinness, O., et al. (2018). Bile diversion, a bariatric surgery, and bile acid signaling reduce central cocaine reward. PLoS Biol *16*, e2006682.
Reichelt, A.C., Westbrook, R.F., and Morris, M.J. (2015). Integration of reward signalling and appetite regulating peptide systems in the control of food-cue responses. Br J Pharmacol *172*, 5225–5238.
Roman, C.W., Derkach, V.A., and Palmiter, R.D. (2016). Genetically and functionally defined NTS to PBN brain circuits mediating anorexia. Nat Commun *7*, 11905.
Rossi, M.A., and Stuber, G.D. (2018). Overlapping Brain Circuits for Homeostatic and Hedonic Feeding. Cell Metab. *27*, 42–56.
Rossi, M.A., Basiri, M.L., McHenry, J.A., Kosyk, O., Otis, J.M., van den Munkhof, H.E., Bryois, J., Hübel, C., Breen, G., Guo, W., et al. (2019). Obesity remodels activity and transcriptional state of a lateral hypothalamic brake on feeding. Science *364*, 1271–1274.
Saper, C.B., Chou, T.C., and Elmquist, J.K. (2002). The need to feed: homeostatic and hedonic control of eating. Neuron *36*, 199–211.
Small, D.M., Jones-Gotman, M., and Dagher, A. (2003). Feeding-induced dopamine release in dorsal striatum correlates with meal pleasantness ratings in healthy human volunteers. Neuroimage *19*, 1709–1715.
Spierling, S., de Guglielmo, G., Kirson, D., Kreisler, A., Roberto, M., George, O., and Zorrilla, E.P. (2020). Insula to ventral striatal projections mediate compulsive eating produced by intermittent access to palatable food. Neuropsychopharmacology *45*, 579–588.
Sutton, L.P., and Caron, M.G. (2015). Essential role of D1R in the regulation of mTOR complex1 signaling induced by cocaine. Neuropharmacology *99*, 610–619.
Sykaras, A.G., Demenis, C., Case, R.M., McLaughlin, J.T., and Smith, C.P. (2012). Duodenal enteroendocrine I-cells contain mRNA transcripts encoding key endocannabinoid and fatty acid receptors. PLoS One *7*, e42373.
Takeuchi, T., Duszkiewicz, A.J., Sonneborn, A., Spooner, P.A., Yamasaki, M., Watanabe, M., Smith, C.C., Fernández, G., Deisseroth, K., Greene, R.W., et al. (2016). Locus coeruleus and dopaminergic consolidation of everyday memory. Nature *537*, 357–362.
Tam, J., Vemuri, V.K., Liu, J., Bátkai, S., Mukhopadhyay, B., Godlewski, G., Osei-Hyiaman, D., Ohnuma, S., Ambudkar, S.V., Pickel, J., et al. (2010). Peripheral CB1 cannabinoid receptor blockade improves cardiometabolic risk in mouse models of obesity. J Clin Invest *120*, 2953–2966.
Tellez, L.A., Medina, S., Han, W., Ferreira, J.G., Licona-Limón, P., Ren, X., Lam, T.T., Schwartz, G.J., and de Araujo, I.E. (2013). A gut lipid messenger links excess dietary fat to dopamine deficiency. Science *341*, 800–802.
Tellez, L.A., Han, W., Zhang, X., Ferreira, T.L., Perez, I.O., Shammah-Lagnado, S.J.,

van den Pol, A.N., and de Araujo, I.E. (2016). Separate circuitries encode the hedonic and nutritional values of sugar. Nat Neurosci *19*, 465–470.

Usiello, A., Baik, J.H., Rougé-Pont, F., Picetti, R., Dierich, A., LeMeur, M., Piazza, P.V., and Borrelli, E. (2000). Distinct functions of the two isoforms of dopamine D2 receptors. Nature *408*, 199–203.

Valjent, E., Biever, A., Gangarossa, G., and Puighermanal, E. (2019). Dopamine signaling in the striatum. In Advances in Protein Chemistry and Structural Biology, (Academic Press), p.

Wang, G.-J., Geliebter, A., Volkow, N.D., Telang, F.W., Logan, J., Jayne, M.C., Galanti, K., Selig, P.A., Han, H., Zhu, W., et al. (2011). Enhanced striatal dopamine release during food stimulation in binge eating disorder. Obesity (Silver Spring) *19*, 1601–1608.

Wang, X.-F., Liu, J.-J., Xia, J., Liu, J., Mirabella, V., and Pang, Z.P. (2015). Endogenous Glucagon-like Peptide-1 Suppresses High-Fat Food Intake by Reducing Synaptic Drive onto Mesolimbic Dopamine Neurons. Cell Rep *12*, 726–733.

Wei, W., Pham, K., Gammons, J.W., Sutherland, D., Liu, Y., Smith, A., Kaczorowski, C.C., and O'Connell, K.M.S. (2015). Diet composition, not calorie intake, rapidly alters intrinsic excitability of hypothalamic AgRP/NPY neurons in mice. Sci Rep *5*, 16810.

Wise, R.A. (2004). Dopamine, learning and motivation. Nat. Rev. Neurosci. *5*, 483–494.

Figure legends

Figure 1: Allostatic adaptations of metabolic efficiency to time-locked access to palatable diet. (**A**) Experimental design. Control animals (Ctr) or bingeing animals (Binge) had daily intermittent access to water or a palatable mixture for 1 hour. Regular chow pellets were provided *ad libitum* throughout the entire experiment. Pictures show the gut of animals after the last binge session. (**B**) Daily binge consumption (ml) of palatable mixture during a 14-days protocol. Statistics: ***p<0.001 Binge *vs* Control. (**C**) 24 hrs locomotor activity in calorimetric chambers (average of 3 consecutive days). Red dotted rectangles indicate the locomotor activity 2 hrs prior and after palatable food access. Statistics: *p<0.05 and **p<0.01 Binge *vs* Control. (**C^{1}**) Cumulative locomotor activity two hours prior and after palatable food access. Results are expressed as beam breaks (bb). Statistics: *p<0.05 and ***p<0.001 Binge *vs* Control. (**D**) Temporal pattern of regular chow food intake (FI, kcal/h) during 24 hrs (average of 3 consecutive days). Statistics: **p<0.01 Binge *vs* Control. (**D^{1}**) Cumulative chow food intake during the dark period. Statistics: ***p<0.001 Binge *vs* Control. (**E**) 24 hrs food intake considering all calories: standard diet (SD) and palatable food (PF). Statistics: ***p<0.001 Binge(SD) *vs* Control(SD), $^{\#\#\#}$p<0.001 Binge(SD+PF) *vs* Binge(SD). Note: standard diet (SD), palatable food (FD). (**F**) Animals' body weight throughout the entire experimental procedure. (**G**) Longitudinal profile of the respiratory energy ratio (RER) from indirect calorimetry (average of 3 consecutive days) and (**G^{1}**) averaged RER values 2 hours prior and after palatable food access. Statistics: **p<0.01 and ***p<0.001 Binge *vs* Control. (**H**) Longitudinal profile of energy expenditure (EE) from indirect calorimetry (average of 3 consecutive days) and (**H^{1}**) averaged EE values 2 hours prior and after palatable food access. Statistics: *p<0.05 and **p<0.01 Binge *vs* Control. (**I**) Brown adipose tissue (BAT) temperature during bingeing. Statistics: *p<0.05 and **p<0.01 Binge *vs* Control. (**J**) Real-time core temperature recording during 24 hrs and (**J^{1}**) averaged values 2 hours prior and after palatable food access. Statistics: ***p<0.001 Binge *vs* Control. (**K**) Matching locomotor activity from core temperature measurements. Statistics: ***p<0.001 Binge *vs* Control. For number of mice/group and statistical details see **Suppl. Table 1**.

Figure 2: Peripheral signals adapt to time-locked access to palatable diet. (**A**) Plasma triglycerides (TG), (**B**) insulin and (**C**) corticosterone levels in animals exposed to water (Control), 1h prior (Anticipation) or 1h after (Consumption) access to palatable diet. Statistics: *p<0.05 and ***p<0.001 Anticipation *vs* Control, $^{\#\#}$p<0.01 Consumption vs Anticipation. (**D**) Blood glucose and (**E**) insulin levels in animals daily exposed to water (Ctr) or palatable diet (binge) after an oral glucose tolerance test (OGTT). Statistics: *p<0.05 Binge *vs* Control only at 30 min post OGTT. (**D^{1}** and **E^{1}**) Glucose and insulin AUC, respectively. For number of mice/group and statistical details see **Suppl. Table 1**.

Figure 3: Binge eating induces dopamine-related molecular modifications. **A.** 1 hour consumption of water (Ctr) or palatable diet (Anticipation, Binge) during the paradigm. On day 14, "acute" animals were exposed to palatable diet for the first time while "anticipation" animals did not receive the food-reward. (**B**) Punches were extracted from the dorsal striatum (DS) and nucleus accumbens (NAc) for western blotting analysis. Phosphorylated ERK1/2, ribosomal protein S6 Ser$^{235/236}$ (P-S6$^{S235/236}$) and phosphorylated ribosomal protein S6 Ser$^{240/244}$ (P-S6$^{S240/244}$) expression in the DS and NAc (**C**). (**D**, **E**) Protein quantification of phospho-ERK, S6$^{S235/236}$ and S6$^{S240/244}$ in the DS (**D**) and NAc (**E**). Statistics: *p<0.05, **p<0.01 and ***p<0.001 Binge or Anticipation *vs* Control. (**F**, **G**) Immunolabeling and quantification of phosphorylated rpS6 in the DS (F) and NAc (G) in control and binge animals. Statistics: ***p<0.001 Binge *vs* Control. For number of mice/group and statistical details see **Suppl. Table 1**.

Figure 4: Binge eating induces dopamine-related modifications in a D1R-dependent manner. (**A, B**) Temporal profile of locomotor activity and cumulative locomotor response (**A^{1}** and **B^{1}**) of animals treated with the dopamine-transport blocker GBR during the anticipatory phase (**A**, **A^{1}**) or one hour after intermittent access to water (Ctr + GBR) or palatable diet (Binge + GBR) (**B**, **B^{1}**). Results are expressed as beam breaks (bb). Statistics: **p<0.01 Binge+GBR *vs* Control+GBR. (**C**) Palatable diet intake after vehicle (Veh+Binge) or D1R antagonist SCH23390 (SCH+Binge) treatment. Statistics: ***p<0.001 SCH+Binge *vs* Veh+Binge. (**D**) Palatable diet intake after vehicle (Veh+Binge) or D2R antagonist haloperidol 0.25 mg/kg or 0.5 mg/kg (H$^{0.25}$+Binge and H$^{0.5}$+Binge) treatment. Immunolabeling of

phosphorylated rpS6 in the DS (**E**) and NAc (**F**) and their associated quantifications (**E^{1}**, **E^{2}**, **F^{1}**, **F^{2}**) in mice pretreated with SCH23390 or vehicle and exposed to time-locked palatable diet. Statistics: ***p<0.001 Veh+Binge *vs* Veh+Control, $^{###}$p<0.001 SCH+Binge *vs* Veh+Binge. (**G**) Temporal profile of locomotor activity and cumulative locomotor response (**G^{1}**) of animals receiving SCH (SCH+Binge) or vehicle (Veh+Binge) (red arrow) and access to palatable diet (black arrow). Statistics: **p<0.01 SCH+Binge *vs* Veh+Binge. (**H**) Cumulative regular chow diet intake following SCH23390 (SCH+Binge) or vehicle (Veh+Binge). Statistics: **p<0.01 SCH+Binge *vs* Veh+Binge. (**I**) Temporal profile of locomotor activity and cumulative locomotor response (2 hrs and 30 min, **I^{1}**) induced by the D1R agonist SKF81297 administered 1 hour after access to time-locked water (Ctr+SKF) or palatable diet (Binge+SKF). Statistics: *p<0.05 and **p<0.01 Binge+SKF *vs* Control+SKF. For number of mice/group and statistical details see **Suppl. Table 1**.

Figure 5: Peripheral endocannabinoids (eCBs) govern binge eating. (**A**) Palatable bingeing in animals pretreated with vehicle (Veh), leptin, insulin, GLP1 agonists exendin-4 (Exe4) and liraglutide (Lira), CCK octapeptide sulfated (CCK-8S) or CB1R inverse agonist AM251. Statistics: ***p<0.001 Exe4-, Lira-, CCK-8S- & AM251-treated Bingeing mice *vs* Veh+Binge mice, $^{###}$p<0.001 AM251-treated *vs* Exe4-, Lira & CCK-8S-treated bingeing mice. (**B**) Dosage of peripheral and circulating endocannabinoids: anadamide (AEA), diacylglycerol (2-AG), docosahexanoyl ethanolamide (DHEA) and oleoylethanolamide (OEA) 1 hour before and 1 hour after palatable bingeing. (**C**) Palatable bingeing in animals pre-treated with a single i.p. injection of vehicle (Veh), peripheral CB1R antagonist AM6545 (10 mg/kg), and/or monoacylglycerol lipase inhibitor JZL184 (8 mg/kg). Statistics: ***p<0.001 AM6545, JZL184, AM6545+JZL184 *vs* Veh-Binge. (**D**) Chronic effect of JZL184 and AM6545 on palatable bingeing. Statistics: ***p<0.001 AM6545-Binge *vs* Veh-Binge, $^{###}$p<0.001 JZL184-Binge *vs* Veh-Binge. (**E**, **F**) Effects of AM6545 on core temperature (**E**) and locomotor activity (**F**). Statistics: **p<0.01 AM6545-Binge *vs* Veh-Binge. Note: black and red arrows indicate administration of AM6545 and palatable food access, respectively. (**G**) Longitudinal measurement of fatty acid oxidation (FAO) following administration of AM6545 during a Binge session and a NoBinge session. (**G^{1}**) Averaged FAO from time of injection (11h00) till the end of light phase (19h00). (**G^{2}**) Ratio of FAO and food intake to discriminate between the

effect of AM6545 and calories intake. Statistics: ***p<0.001 AM6545 *vs* Veh (in both Binge and NoBinge sessions). (**H**) Palatable bingeing after oral gavage of AM6545 (10 mg/kg, p.o.) and associated fatty acids oxidation (**I**). (**J**) The scheme indicates gut-originated afferent paths that were virally targeted to perform single-cell transcriptomic analysis (Bai et al., 2019). (**K**) Enrichment of different vagal markers (*SLC17a6*, *Scn10a*, *Htr3a*, *Cartpt*, *Grin1*, *Phox2b*) and comparison with *Cnr1* and *Cnr2* in sensory vagal neurons labeled from microinjections in the stomach, proximal and middle intestines. For number of mice/group and statistical details see **Suppl. Table 1**.

Figure 6: The gut-brain vagal axis is required for eCBs-mediated effects. (**A**, **B**) cFos immunolabeling in the area postrema (AP), the nucleus tractus solitarius (NTS), the lateral parabrachial nucleus (lPBN) and medial parabrachial nucleus (mPBN) in sham and vagotomized animals treated with the peripheral CB1R antagonist AM6545 (10 mg/kg). (**A^{1}**) Scheme indicates the central vagus→NTS→PBN→target regions path in VGX mice. (**A^{2}**) Quantification of cFos-positive neurons in the AP, NTS and lPBN in sham and VGX mice injected with AM6545. Statistics: ***p<0.001 VGX+AM6545 *vs* Sham+AM6545. (**B**) Palatable bingeing in sham and vagotomized (VGX) animals pre-treated with AM6545 (A) or vehicle (V), and associated measurements of fatty acid oxidation (**C, C^{1}** and **D, D^{1}**). Statistics: ***p<0.001 Sham+AM6545 *vs* Sham+Veh. (**E**) cFos immunolabeling of paraventricular nucleus of the hypothalamus (PVN) and dormomedial nucleus of the hypothalamus (DMH) in sham or VGX animals treated with vehicle or AM5646 and associated counting (**E^{1}**). Statistics: ***p<0.001 Sham+AM6545 *vs* Veh, $^{###}$p<0.001 VGX+AM6545 *vs* Sham+AM6545. For number of mice/group and statistical details see **Suppl. Table 1**.

Figure 7: Peripheral CB1R signaling routed by the vagus nerve controls VTA DA-neurons activity. (**A, A^{1}**) Effect of AM6545 or Veh on GBR-induced locomotor activity (beam breaks, bb). Statistics: **p<0.01 AM6545+GBR *vs* Veh+GBR. (**B**, **B^{1}**) Effect of AM6545 on GBR-triggered cFos in the striatum. Statistics: ***p<0.001 AM6545+GBR *vs* Veh+GBR. (**C**) Amphetamine (Amph)-induced locomotor activity and (**C^{1}**) cumulative locomotor response (**C1**) in mice pretreated with vehicle (Veh+Amph) or AM6545 (AM6545+Amph). GBR-induced locomotor activity (**D**),

cumulative locomotor response (**D**[1]) in VGX mice pretreated with vehicle (VGX/Veh+GBR) or AM6545 (VGX/AM6545+GBR). GBR-induced locomotor activity (**E**) and cumulative locomotor response (**E**[1]) in mice pretreated with oral gavage of vehicle (Veh (po)+GBR) or AM6545 (AM6545 (po)+GBR). (**F**) Expression of GCaMP6f in VTA dopamine neurons of virally injected *Drd2*-Cre mice. Please, note colocalization with TH and GCaMP6f-positive terminals in the striatum and NAc. (**G**) Behavioral paradigms used to trigger the activity of VTA dopamine neurons: exposure to a new environment (new cage) and tail suspension. (**H**) Temporal dynamics of DA-neurons activity during the exposure to a new environment (new cage). Statistics: **p<0.01 AM6545 *vs* Veh. (**I**) Temporal dynamics of DA-neurons activity during the tail suspension test. Statistics: **p<0.01 AM6545 *vs* Veh. For number of mice/group and statistical details see **Suppl. Table 1**.

Supplemental Figure 1: Adaptations to time-locked palatable feeding. (**A**) Binge consumption and (**B**) time to first lick during the last BE session of milkshake (lipids+sucrose), sucralose (2 mM) and saccharin (0.1% w/v). Statistics: ***p<0.001 Sucralose or Saccharin *vs* Milkshake (Lipids/Sucrose). Body composition [fat mass, (**C**) and lean mass (**D**)] of control and bingeing mice. (**E**) Longitudinal profile of the fatty acids oxidation (FAO) from indirect calorimetry measurements (average of 3 consecutive days). For number of mice/group and statistical details see **Suppl. Table 1**.

Supplemental Figure 2: Peripheral CB1R and vagal afferents. (**A**) Longitudinal measurement of fatty acid oxidation (FAO) following oral administration of AM6545 (10 mg/kg). Note no modification in FAO. (**B**, **C**) Expression of *Cnr1* in sensory vagal neurons labeled from microinjections in the distal and large intestines. For number of mice/group and statistical details see **Suppl. Table 1**.

Supplemental Figure 3: Homeostatic adaptations in sham and VGX mice during time-locked palatable feeding. (**A**) 24 hours measurement of chow food intake in sham and VGX bingeing mice. Statistics: ***p<0.001 VGX+Binge *vs* Sham+Binge. (**B**) Body weight of both experimental groups. (**C-E**) Respiratory exchange ratio (RER), fatty acids oxidation (FAO) and energy expenditure (EE) in sham and VGX

mice during a binge session. Statistics: *p<0.05, **p<0.01 VGX+Binge *vs* Sham+Binge. For number of mice/group and statistical details see **Suppl. Table 1**.

Supplemental Figure 4: *In vivo* recoding of Ca^{2+} transients in VTA dopamine neurons of *Drd2*-Cre mice. (**A**) Ca^{2+} transients evoked following presentation of a high-fat high-sugar (HFHS) pellet (positive and reinforcing stimulus). Statistics: ***p<0.001 $HFHS_{after}$ *vs* $HFHS_{before}$. (**B**) Ca^{2+} transients evoked following scruff restraint (negative stimulus). Note: artefact signals while restraining the mouse were not included in the analysis. Statistics: ***p<0.001 $Scruff_{after}$ *vs* $Scruff_{before}$. For number of mice/group and statistical details see **Suppl. Table 1**.

Graphical Abstract Berland et al.,

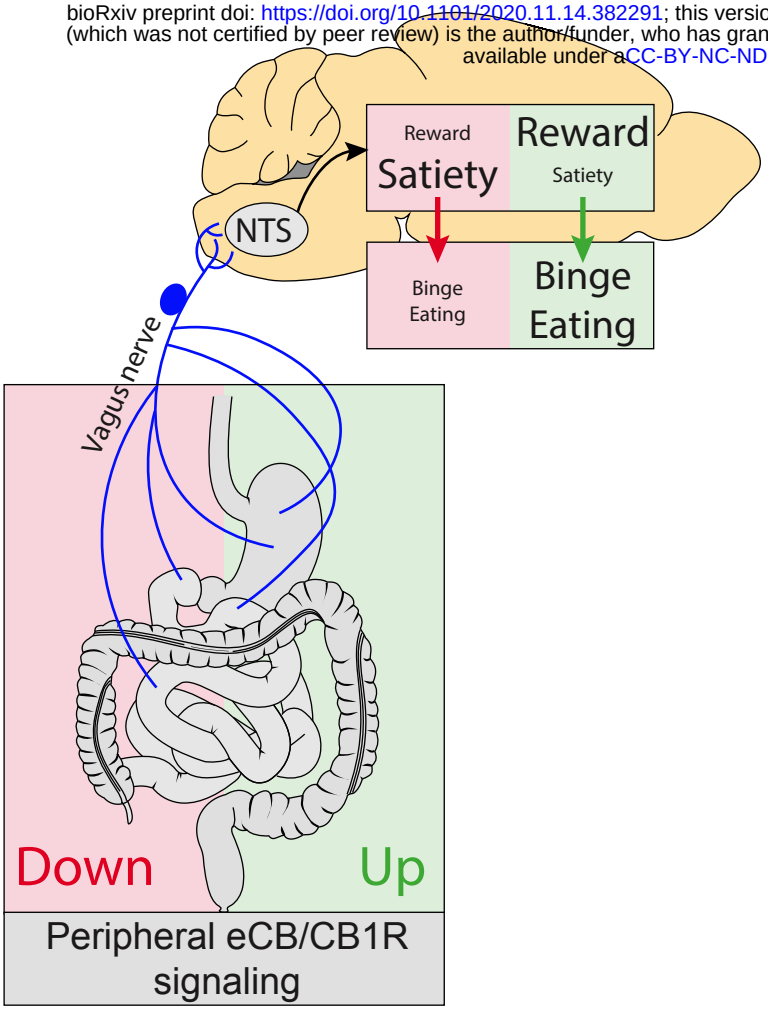

Figure 1 Berland et al.,

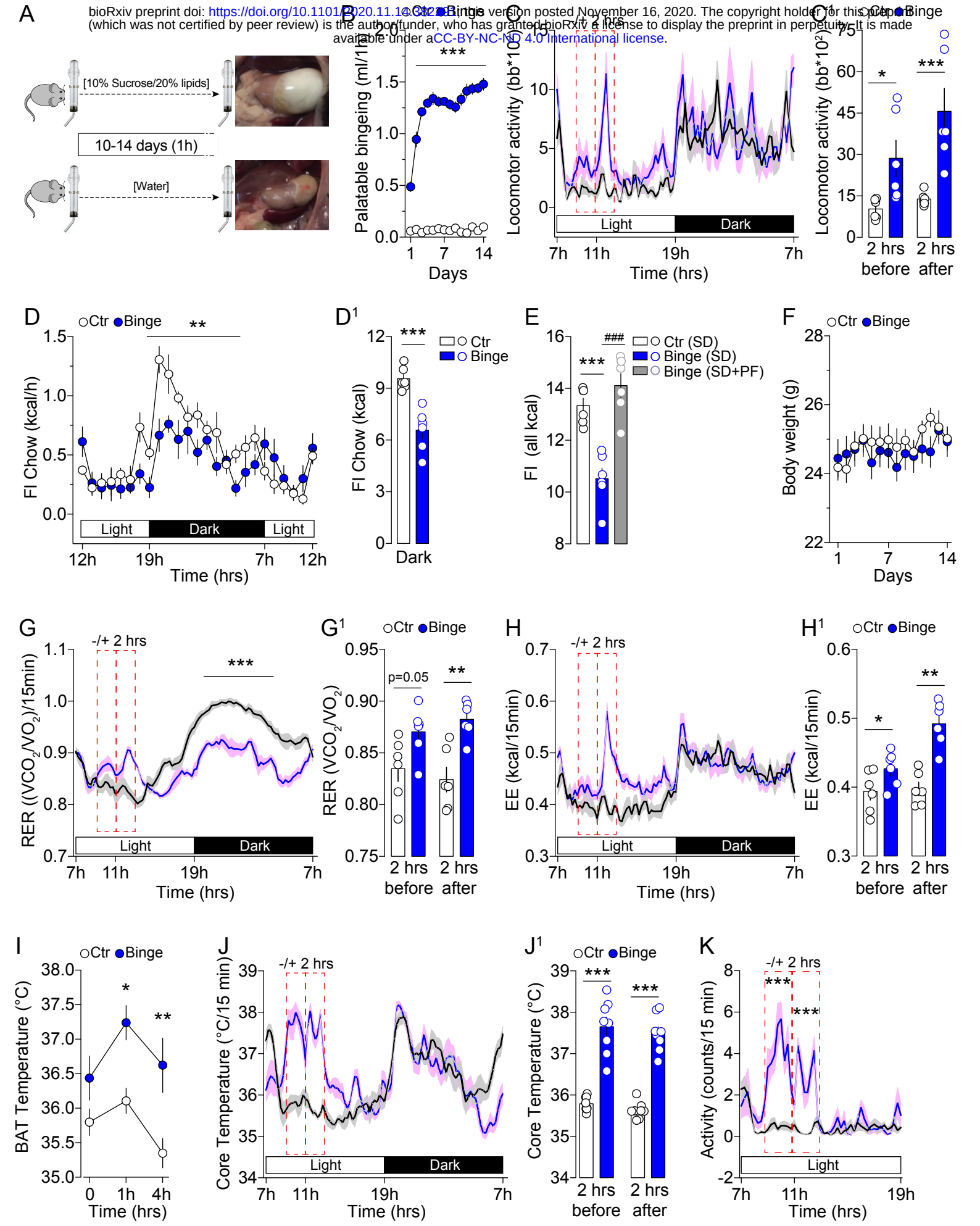

Figure 2 Berland et al.,

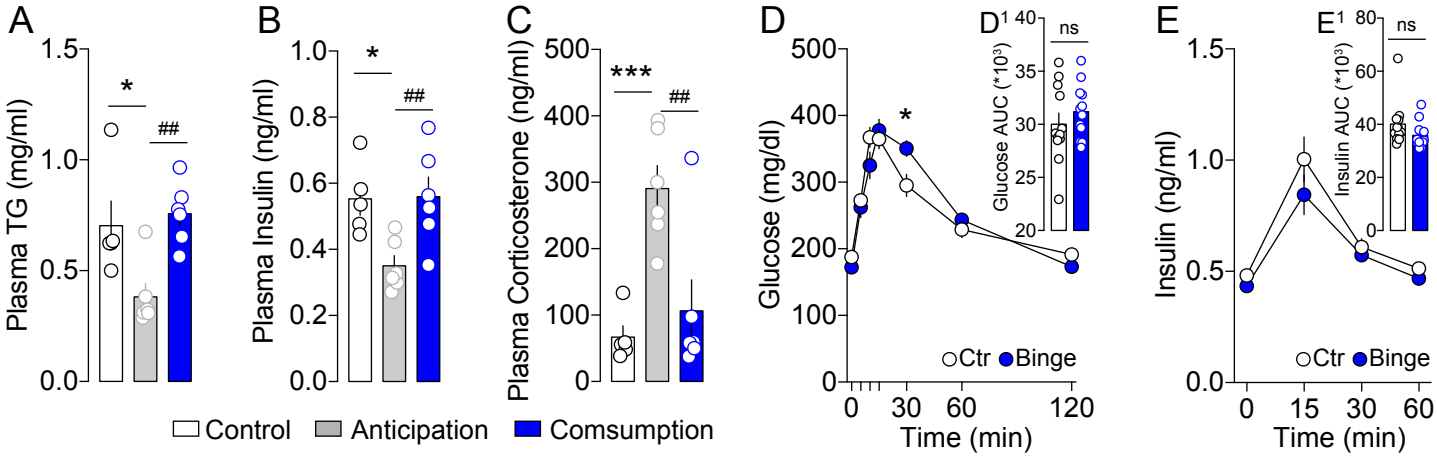

Figure 3 Berland et al.,

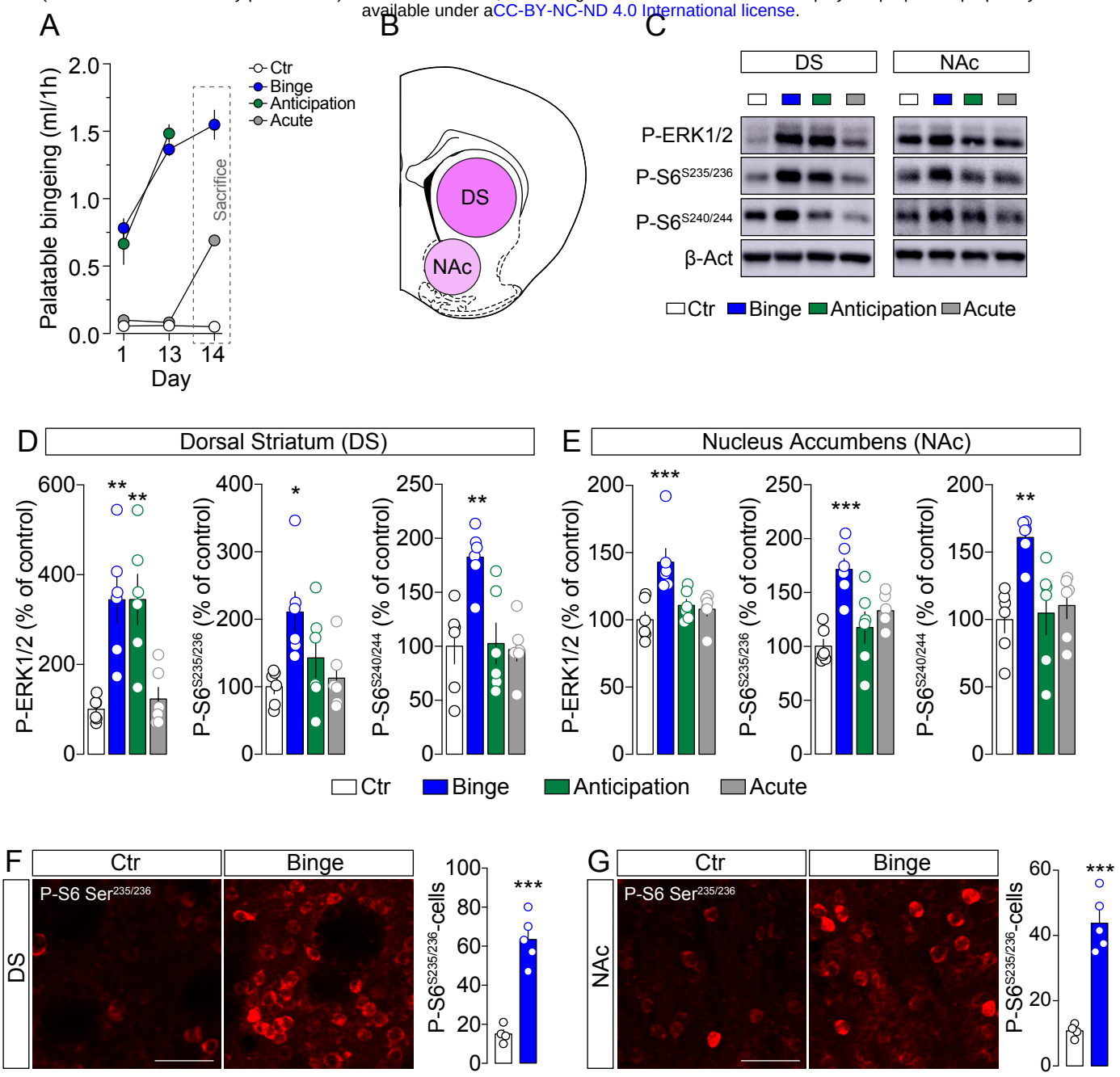

Figure 4 Berland et al.,

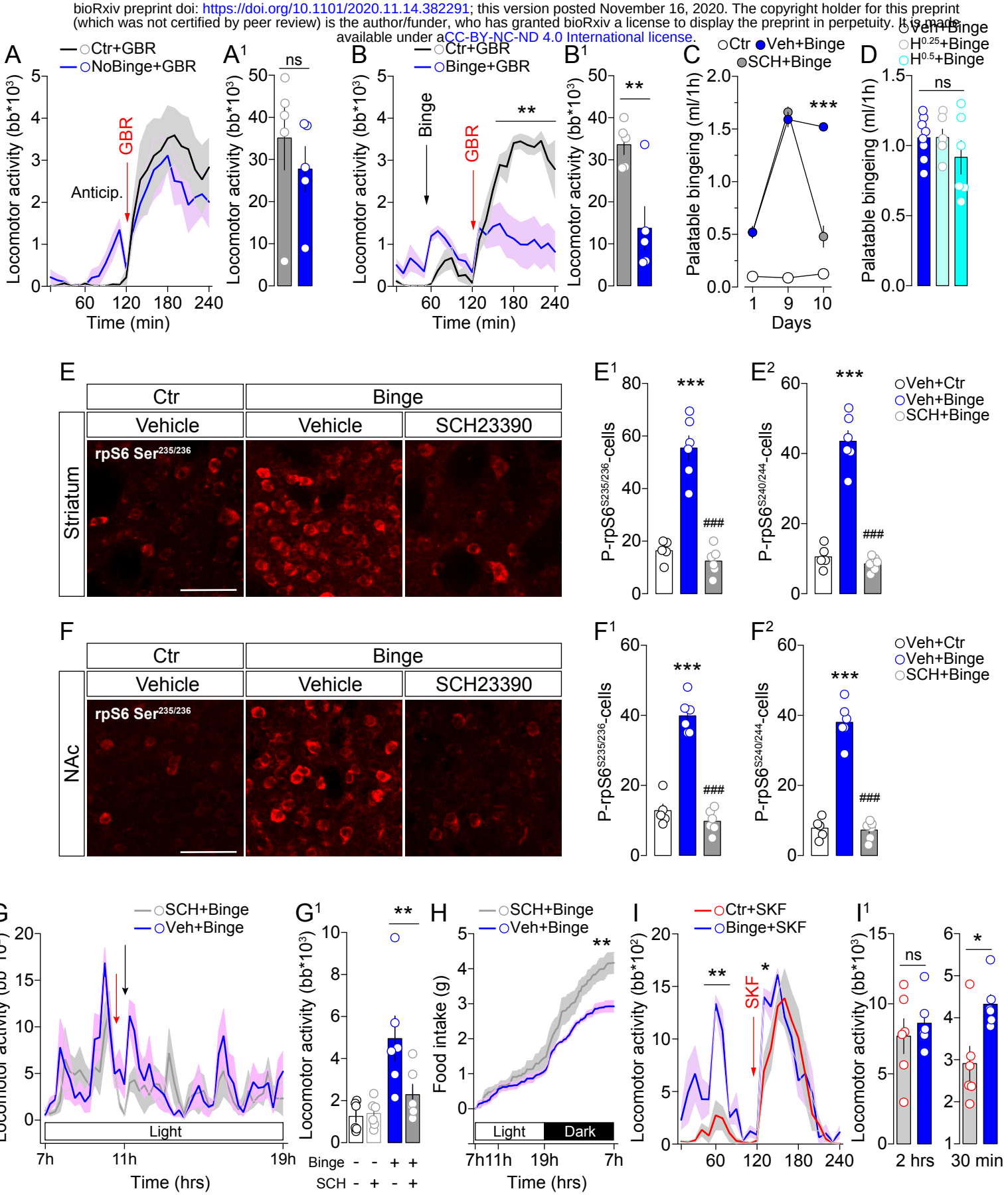

Figure 5 Berland et al.,

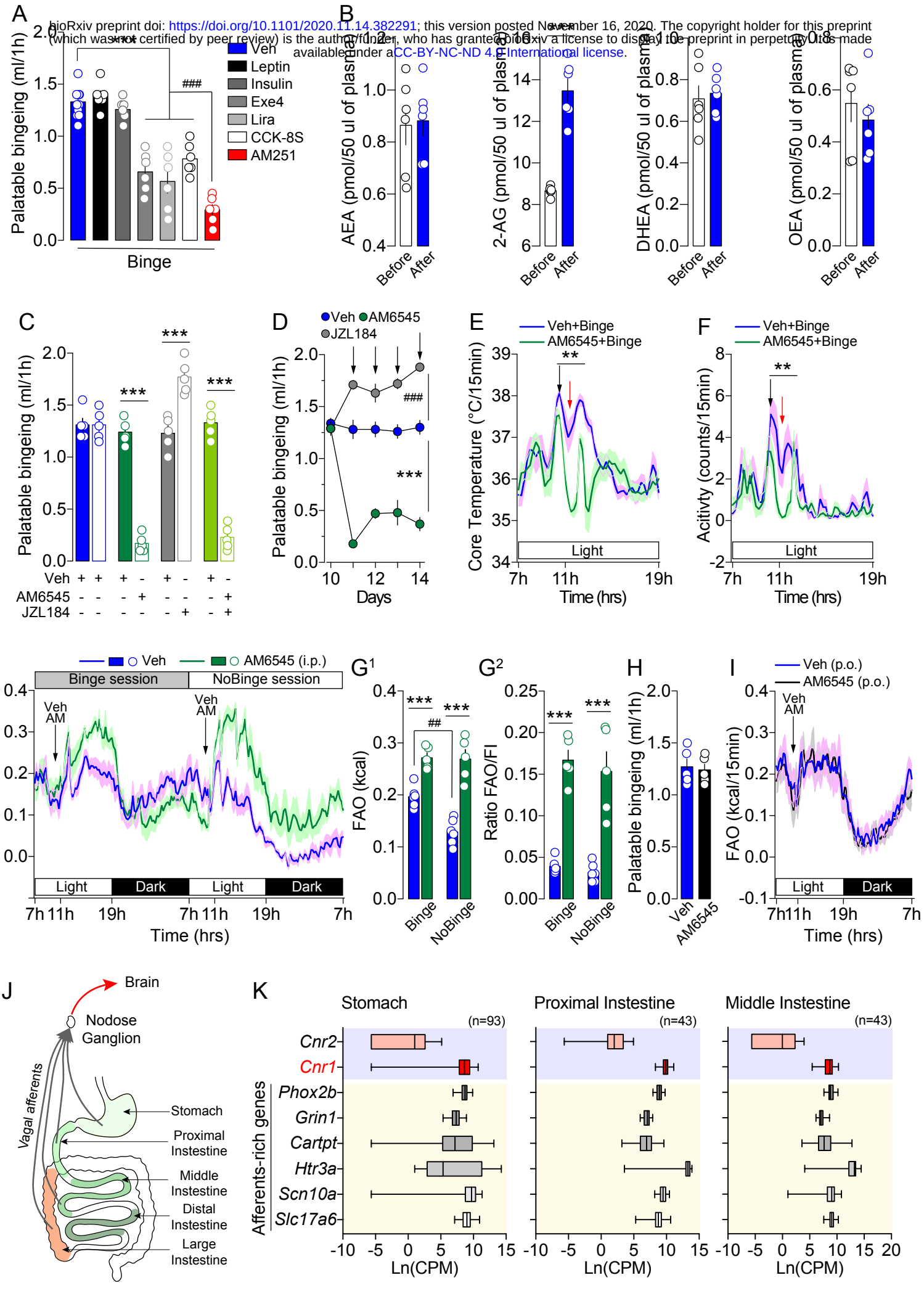

Figure 6 Berland et al.,

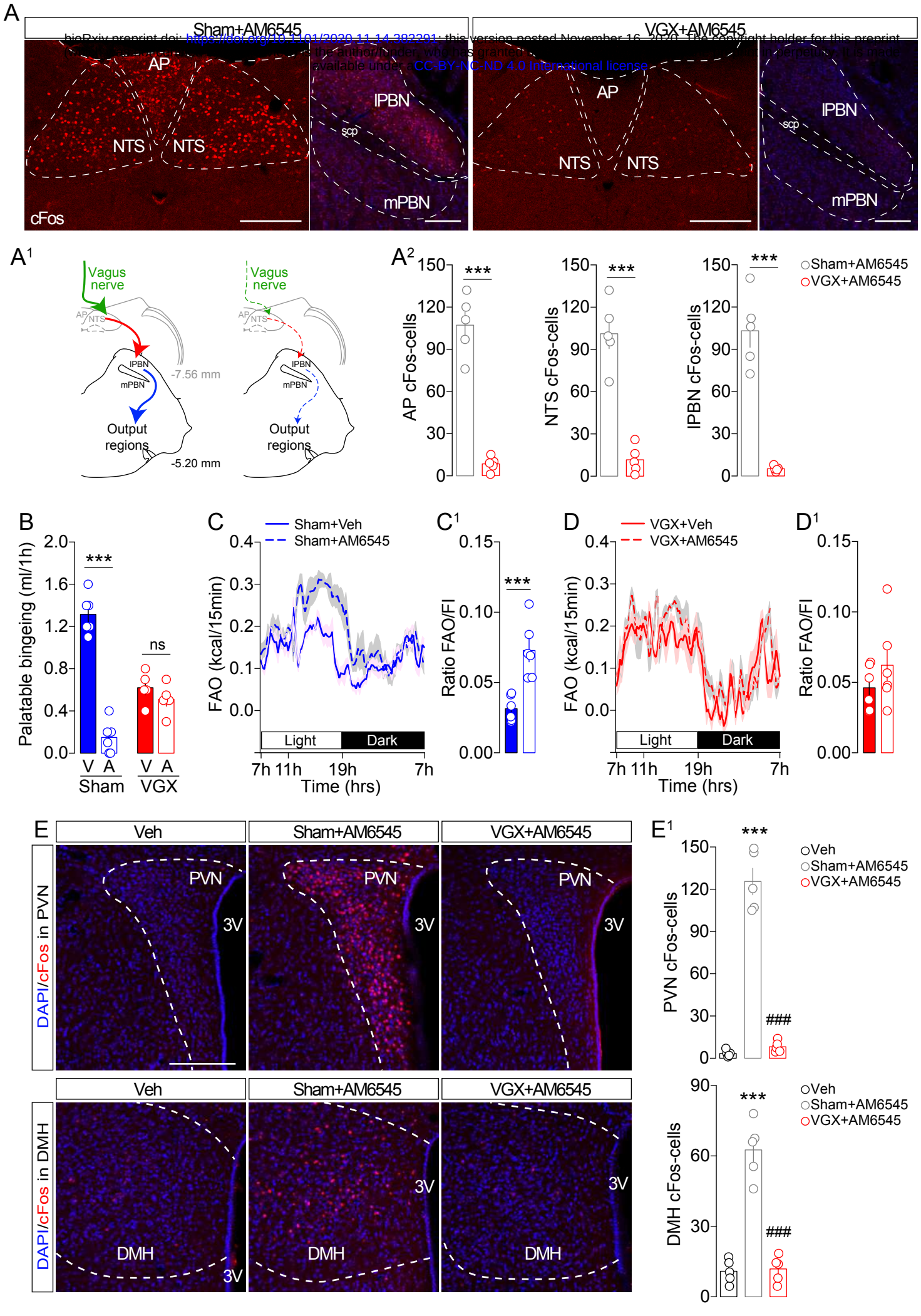

Figure 7 Berland et al.,

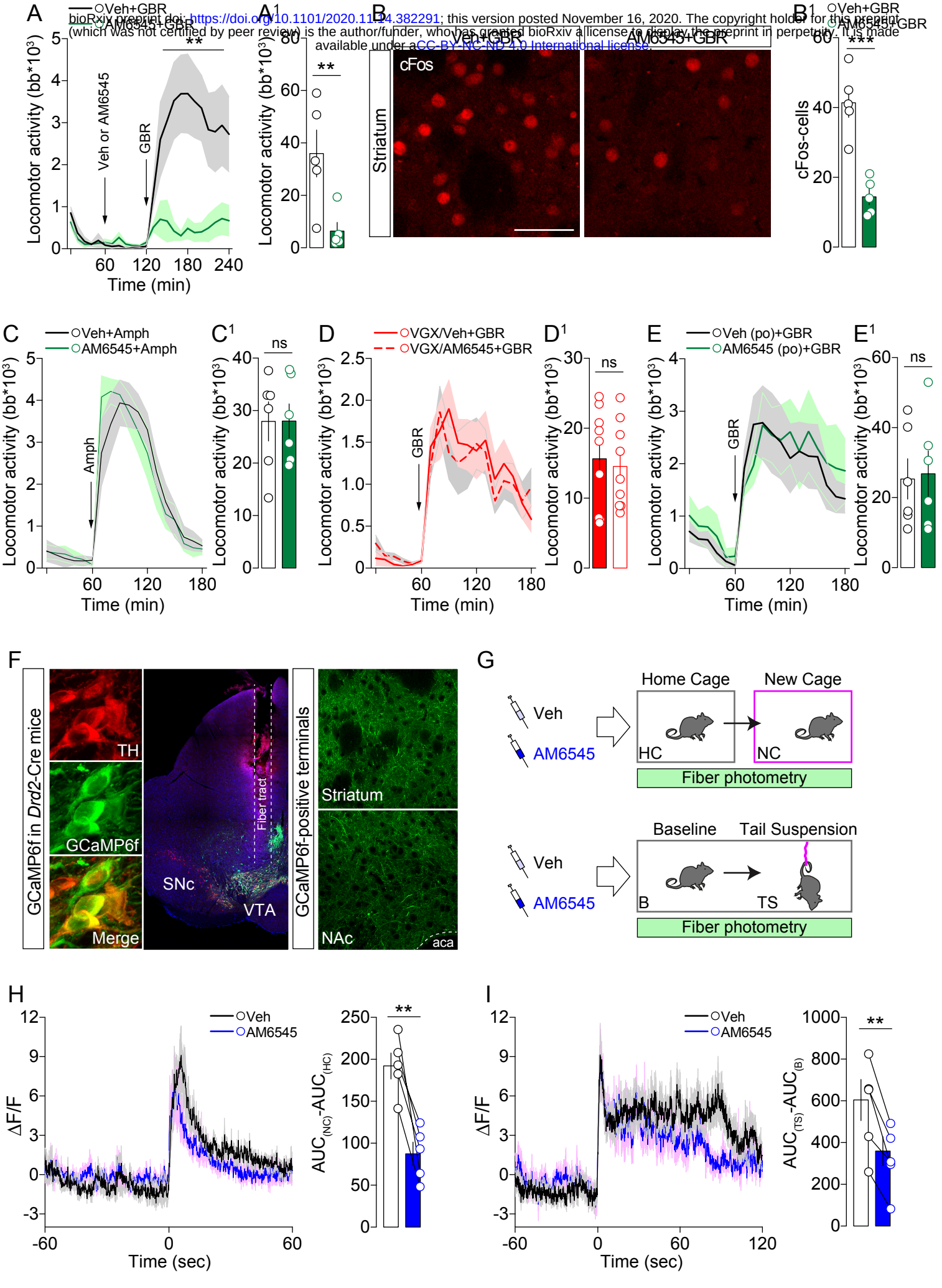

Suppl. Figure 1 Berland et al.,

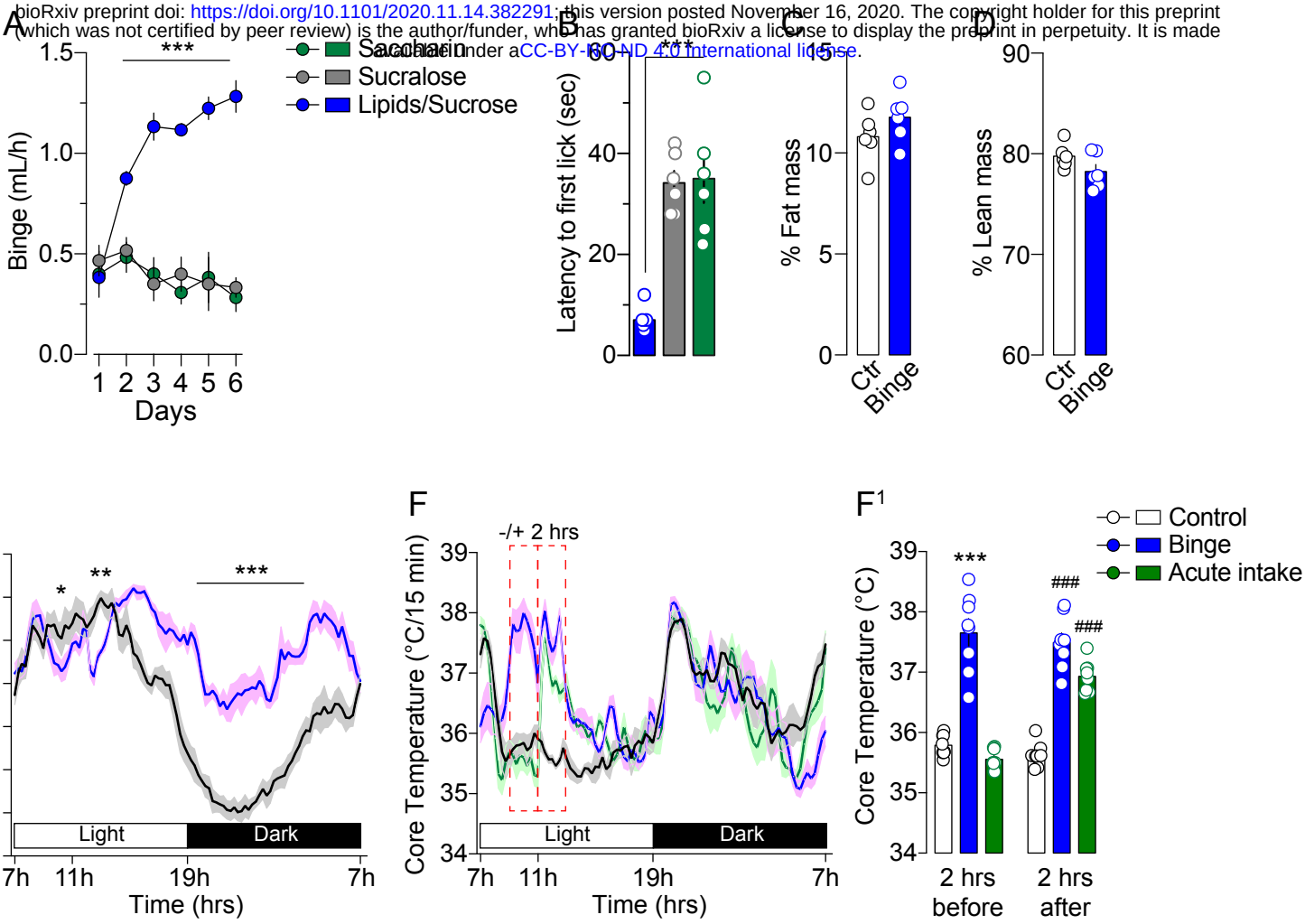

Suppl. Figure 2 Berland et al.,

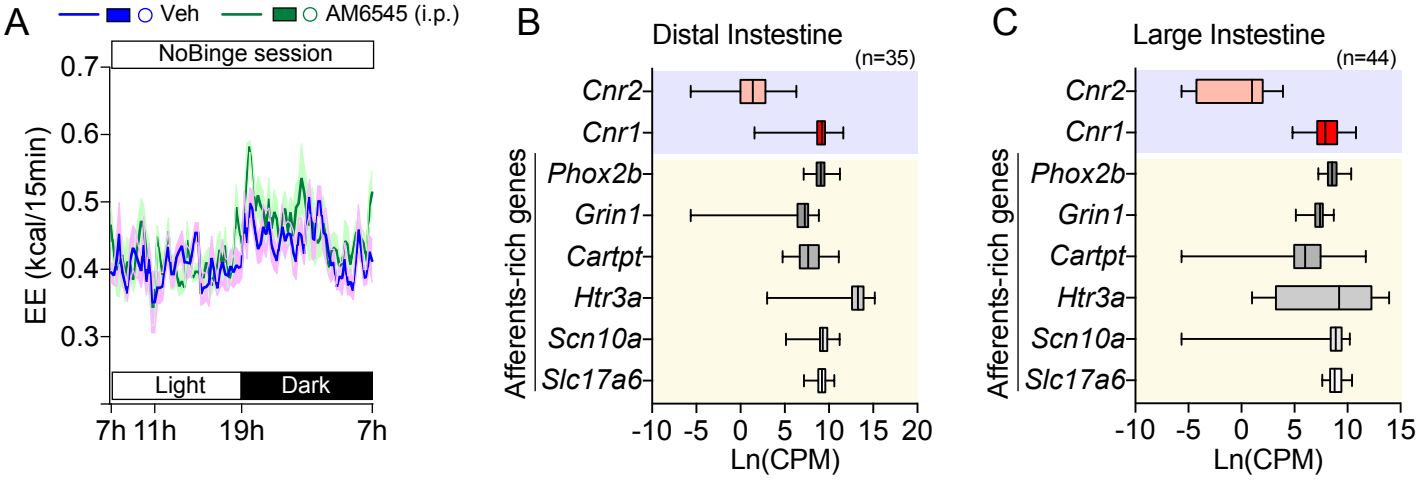

Suppl. Figure 3 Berland et al.,

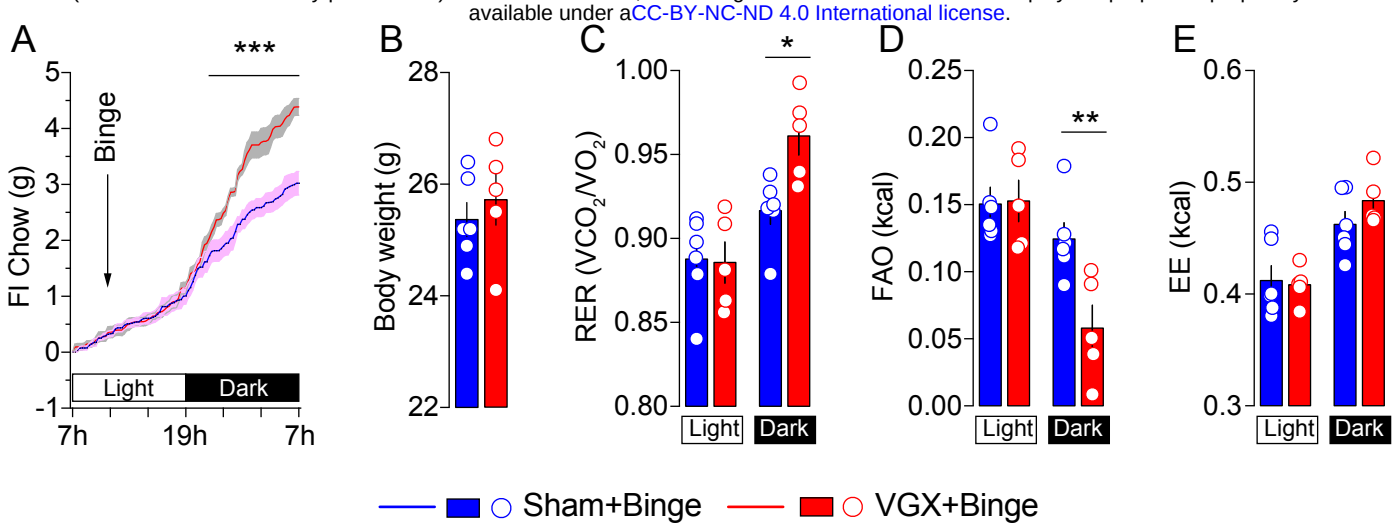

Suppl. Figure 3 Berland et al.,